Journal Pre-proof

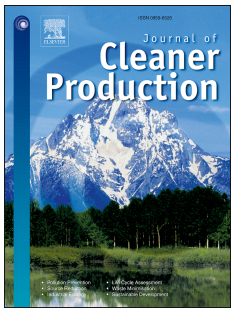

An Equation-Based Multiphysics Modelling Framework for Oxidative Ageing of Asphalt Pavements

Eman L. Omairey, Ph.D. Candidate, Fan Gu, Ph.D, Yuqing Zhang, Ph.D

PII: S0959-6526(20)34446-2

DOI: https://doi.org/10.1016/j.jclepro.2020.124401

Reference: JCLP 124401

To appear in: *Journal of Cleaner Production*

Received Date: 13 May 2020

Revised Date: 28 August 2020

Accepted Date: 23 September 2020

Please cite this article as: Omairey EL, Gu F, Zhang Y, An Equation-Based Multiphysics Modelling Framework for Oxidative Ageing of Asphalt Pavements, *Journal of Cleaner Production*, https://doi.org/10.1016/j.jclepro.2020.124401.

To Journal of Cleaner Production,
12 May 2020

Credit Author Statement

Re: submission of paper entitled "An Equation-Based Multiphysics Modelling Framework for Oxidative Ageing of Asphalt Pavements" by Eman L. Omairey, Fan Gu, and Yuqing Zhang to Journal of Cleaner Production.

The authors confirm contribution to the paper as follows: simulation work, data collection and analysis, and paper draft: Eman Omairey; paper draft, data collection, and paper review: Fan Gu; study conception, objective design, and paper review: Yuqing Zhang. All authors reviewed the results and approved the final version of the manuscript.

All authors interpreted and reviewed the results and approved the manuscript.

Sincerely yours,

Signed by Corresponding Author on behalf of all authors.
Yuqing Zhang, PhD
Senior Lecturer in Highway Engineering
Aston Institute of Materials Research (AIMR)
Engineering System & Management (ESM)
Aston University
Address: Aston Triangle, Birmingham, B4 7ET, U.K.
Tel: +44 121-204-3391
Email: y.zhang10@aston.ac.uk

An Equation-Based Multiphysics Modelling Framework for Oxidative Ageing of Asphalt Pavements

Eman L. Omairey, Ph.D. Candidate
Aston Institute of Materials Research, Aston University
Aston Triangle, Birmingham, B4 7ET (United Kingdom)
Email: omaireye@aston.ac.uk

Fan Gu*, Ph.D.
Former Marie Curie Research Fellow
Aston Institute of Materials Research, Aston University
Aston Triangle, Birmingham, B4 7ET (United Kingdom)
Email: tracygufan@gmail.com
* *Corresponding Author*

Yuqing Zhang*, Ph.D.
Senior Lecturer in Highway Engineering
Aston Institute of Materials Research, Aston University
Aston Triangle, Birmingham, B4 7ET (United Kingdom)
Email: y.zhang10@aston.ac.uk
* *Corresponding Author*

Word Count: 12,271

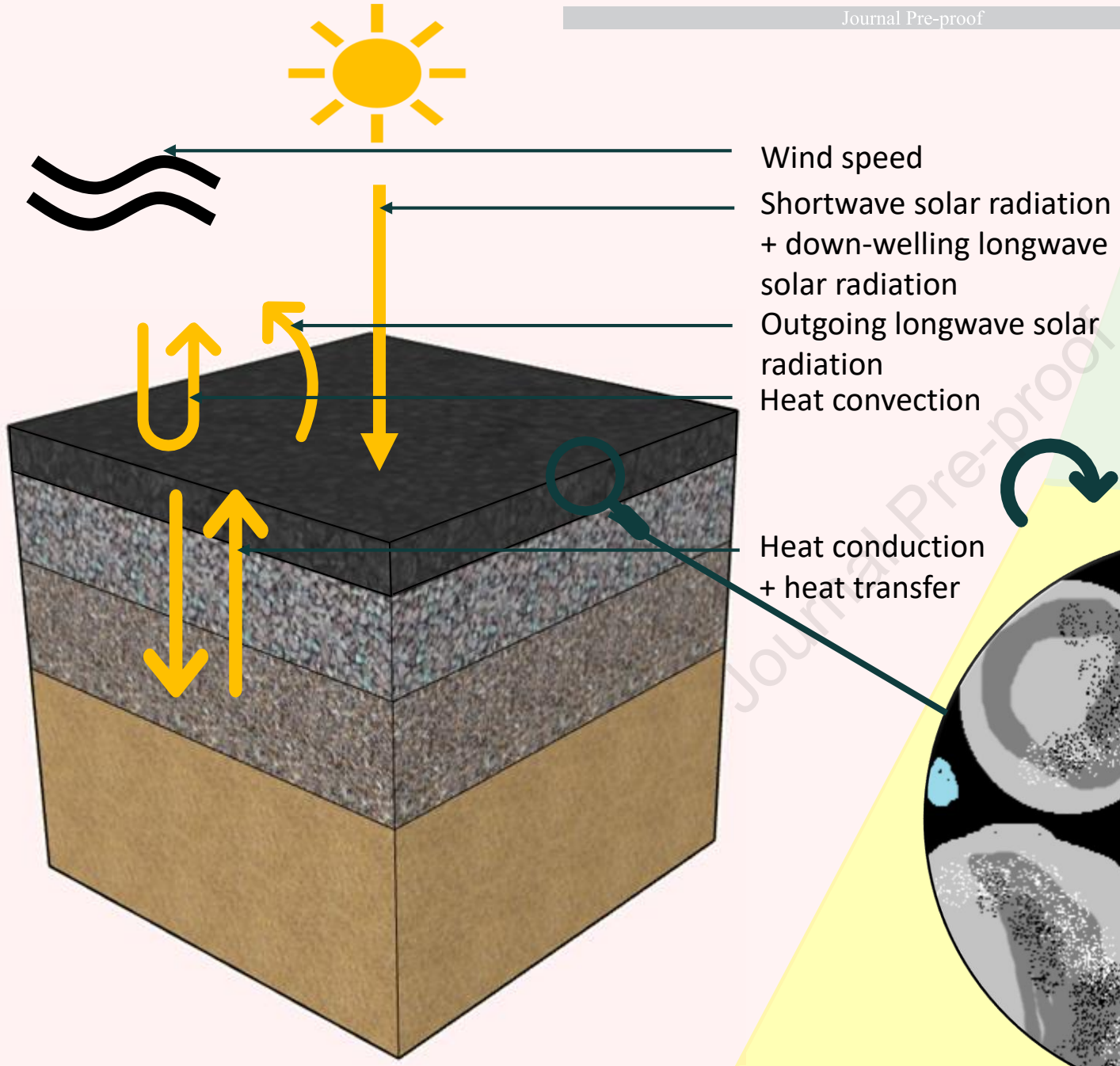

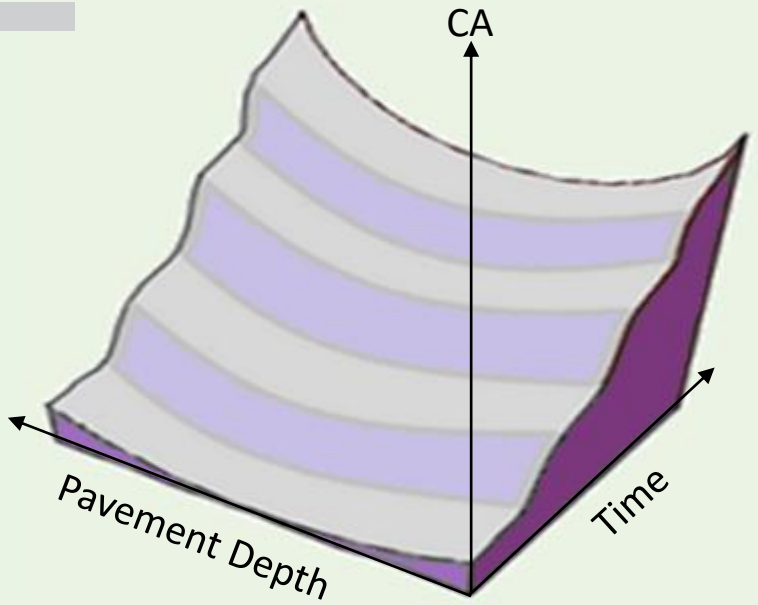

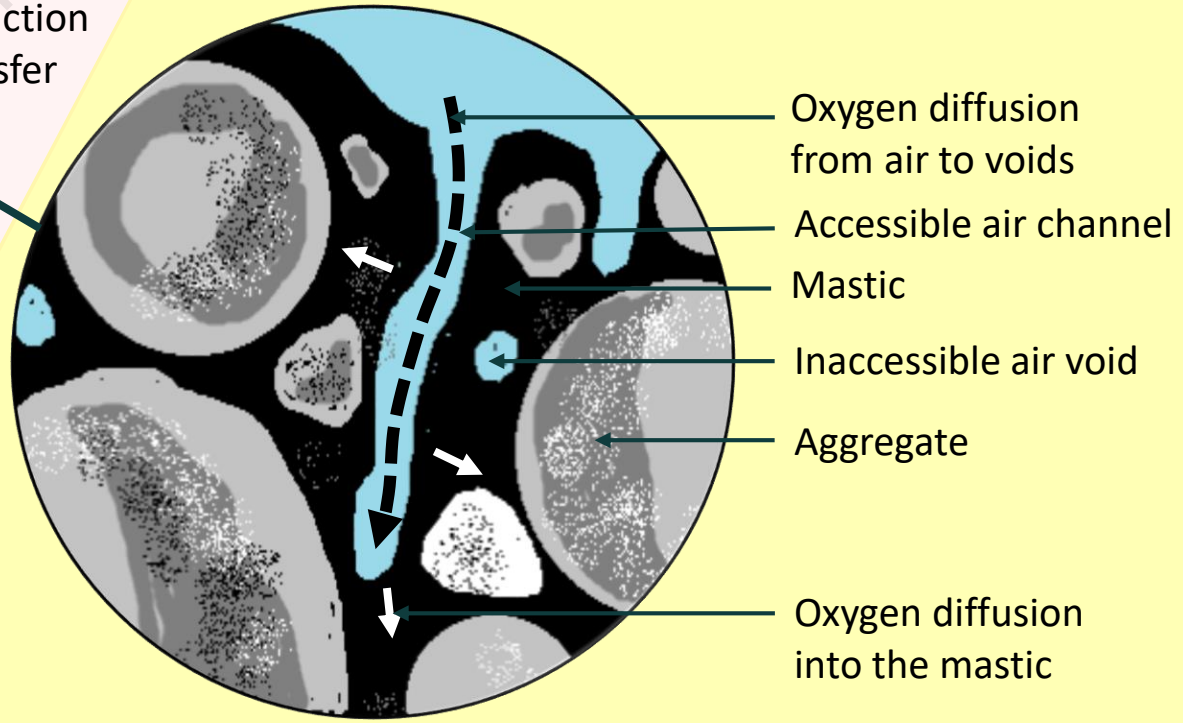

An Equation-Based Multiphysics Modelling Framework for Oxidative Ageing of Asphalt Pavements

Eman L. Omairey, Fan Gu*, and Yuqing Zhang*

Aston Institute of Materials Research, Aston University
Aston Triangle, Birmingham, B4 7ET (United Kingdom)
*Corresponding Author, y.zhang10@aston.ac.uk

Abstract Long-term oxidative ageing occurs in asphalt pavements when they are exposed to the ambient environment for extended periods. This ageing phenomenon is dependent on multiple physical fields, including heat transfer, oxygen diffusion from air into interconnected air voids of asphalt pavement, oxygen diffusion from air void channels to asphalt mastic inside, and growth of oxidation products in bitumen. Most existing oxidative ageing models were established via coupling of limited physical fields. However, to accurately determine the oxidative ageing effect on pavement performance, there is a need to develop a multiphysics model that integrates all ageing-related physical fields comprehensively. The challenge lies in that the ageing-related physics are circularly dependent, time-dependent and highly nonlinear. This study developed a multiphysics and time-dependent finite element model that successfully addressed the issues of high nonlinearity and circular dependency of oxidative ageing in the asphalt pavements.

Specifically, a differential equation-based approach was employed to efficiently couple the multiple physical fields into one integrated model. The multiphysics framework included a pavement temperature prediction model and an integrated ageing model. The model involved a variety of inputs such as site-specific hourly climate data, parameters for oxidation kinetics of bituminous binder, volumetric properties of asphalt mixture, thermal and diffusive properties of pavement materials, and pavement structure. The pavement temperature model was validated using the pavement temperature profiles for different climate regions in the Long-Term Pavement Performance (LTPP) database. The integrated ageing model was validated using the Fourier-transform infrared spectroscopy (FTIR) data of field-aged asphalt cores in the literature. Results showed that the model can accurately predict the change in pavement temperature profile on an hourly basis and reliably predict the degree of oxidative ageing across pavement depth for different climate zones.

Keywords: Long-term Oxidative Ageing, Multiphysics Modelling, Oxidation Kinetics, Oxygen Transport, Heat Transfer.

1 Introduction

Bitumen-based construction materials, including bituminous binders and asphalt mixtures, are mainly used for the surface paving of roads and highways. Bitumen is an extremely complex compound with thousands of different types of hydrocarbons, paraffins, aromatics, and naphthenic compounds. These compounds have various saturations, polarity, functional groups, and heteroatoms. The differing chemical composition of bitumen results in the variation of its mechanical behaviour [1, 2]. Existing studies demonstrated that the chemical composition of bitumen changes with ageing, which occurs in two phases, i.e., short- and long-term ageing [3, 4]. Short-term ageing occurs during the initial construction phase due to volatilisation, oxidation, and absorption of oily components in the maltenes during mixing. Long-term ageing occurs in the pavement service stage and is mainly due to the oxidation process. This study focuses on modelling the long-term oxidative ageing of asphalt materials, which starts after exposing asphalt pavements to the natural environment.

Oxidative ageing is the reaction between asphalt constituents and atmospheric oxygen. The Fourier-transform infrared spectroscopy (FTIR) test is usually employed to identify the change in chemical composition of bitumen due to ageing. According to existing FTIR studies, the oxidative ageing of bitumen causes the formation of carbonyl (C=O) and sulfoxide (S=O) functional group compounds [5-8]. Moreover, the formed carbonyl is much greater than the sulfoxides in terms of product quantity. Therefore, many researchers utilised the formation of carbonyl solely to characterise the change in chemical composition of bitumen in the oxidative ageing process [7, 9, 10]. They determined the carbonyl area (CA) from the FTIR tests to quantify the oxidative ageing of bitumen. While doing so, they found that such a parameter was well correlated to ageing time, ageing temperature and oxygen pressure. In addition to changes in chemical composition, the rheological properties of bitumen (e.g., viscosity and dynamic shear modulus) also exhibit hardening characteristics in the oxidative ageing process. The hardening leads to an increase in these properties so that the asphalt material becomes stiffer and more brittle. Many laboratory and field studies confirmed that the oxidative ageing of asphalt materials leads to the degradation of their physical, chemical, and mechanical properties. This deterioration of the materials and distresses in the pavement

structures eventually resulting in the reduction of pavement durability. Thus, a comprehensive understanding and reliable prediction of the oxidative ageing performance of asphalt pavements is needed.

There are many existing studies focused on the oxidative ageing of asphalt pavements. They can be categorised into four groups according to the various physical fields involved in pavement ageing: oxidative kinetics, morphology influences, environmental effects on ageing, and ageing effects on mechanical responses.

Oxidative kinetics of bitumen and asphalt: Liu et al. (1996) and Peterson and Harnsberger (1998) found that bitumen typically oxidises in two stages, a nonlinear fast-rate period and a linear constant-rate period [9, 11]. To quantify this phenomenon, Jin et al. (2011) developed a two-reaction kinetics model, which could predict the CA of bitumen in various oxidative ageing conditions [10]. Luo et al. (2015, 2019) extended this model to predict the stiffness change of aged asphalts in the field [12, 13]. They found that the activation energy of asphalt pavement was comparable to that of bitumen.

Morphology influences on oxidative ageing: Peterson (2009) and Abu Al-Rub (2013) reported that oxygen diffuses inside asphalt pavement through the interconnected air voids in the asphalt layer [5, 14]. Lower air void contents result in lower oxygen diffusivity, which will reduce the degree of oxidative ageing. Yin et al. (2017) performed the tensile stiffness test on 30 field-aged asphalt samples with different air void contents and then extracted the bitumen to conduct rheology testing. They observed that less hardening occurred in the asphalt sample with a lower interconnected air void content [15].

Environmental effects on ageing: Environmental factors affect oxygen transport and diffusion as well as pavement temperature profile, which further impacts oxidative ageing. To predict asphalt oxidation in pavements, Prapaitrakul et al. (2009) developed an oxygen transport model, which involved oxygen pressure, oxygen concentration, oxygen diffusivity, and pavement temperature [16]. Jin et al. (2013) found that oxygen diffusivity in transport media was related to the temperature and viscosity of the material [17]. Lytton et al. (1993) developed a one-dimensional heat transfer model, the Enhanced Integrated Climate Model (EICM), to calculate heat conduction in asphalt pavements [18]. He assumed a constant-temperature boundary condition (BC) well below the pavement surface. The required climatic inputs included solar radiation, ambient temperature, wind speed, pavement albedo, pavement emissivity, and thermal diffusivity. Han et al. (2011) improved the prediction accuracy of the EICM by taking into account the unsteady-state heat flux boundary condition [19]. The modified heat transfer model was validated by comparing prediction results to measured temperature data from 29 pavement sites across the United States.

Ageing effects on mechanical responses: Lu and Isacsson (1998, 2002), Wang et al. (2014) and Jing et al. (2019) found that oxidative ageing increased the complex shear moduli and decreased the phase angles of both unmodified and polymer-modified bitumen [20 - 23]. Ruan et al. (2003) reported that oxidative ageing also increased the viscosity of bitumen [24]. Existing studies found that the field-aged viscosity of bitumen had a gradient across pavement depth with a higher value near the pavement surface [3, 12]. This phenomenon indicated a non-uniform ageing process occurred in asphalt pavement, which was attributed to the non-uniform distribution of pavement temperature and air void content across pavement depth. Moreover, many prediction models for the mechanical performance of asphalt pavements formulated using performance-related material properties were generated for asphalt pavements at various conditions [14, 25, 26].

The intensive literature review indicates the multiphysics nature of oxidative ageing of asphalt pavements. Specifically, ageing of asphalt materials involves three multiphysics: 1) chemical oxidation reaction in the bitumen; 2) mechanical responses (e.g., altered viscosity); and 3) physical environmental processes (i.e., heat transfer and oxygen diffusion) leading to varying environmental profiles within pavements. These processes are influenced by the microstructural morphology including asphalt film thickness, pore size and air void distribution. However, most of the existing studies only focused a “one physics” approach, ignoring the interaction among these physics, when in fact, the interrelationships among them are circularly dependent in the dynamic ageing process. For example, oxygen distribution affects the chemical oxidation of bitumen, resulting in increased viscosity and decreased diffusivity, which in turn affects oxygen distribution and oxidative ageing. Ignoring the multiphysics nature of oxidative ageing leads to simplification in modelling, thereby reducing the prediction accuracy. Thus, oxidative ageing of asphalt pavements should be modelled in a multiphysics perspective, so that the dynamic circular dependencies among these physics are solved simultaneously for an accurate prediction of ageing in the asphalt pavements. In addition, the multiphysics modelling is capable of assessing the influences of different material and environmental components on oxidative ageing of asphalt pavements from both physical and chemical perspectives.

The multiphysics nature of ageing has been well characterised by ageing theories and field measurement data, as shown in the above studies. However, applying multiphysics models in ageing predictions, considering their circular- and time-dependency, is limited due to some restrictions in Finite Element (FE) modelling. Such restrictions include non-user-friendly interfaces, limited modelling abilities, and restrictions on specific constitutive models. Additionally, user-defined subroutines must be programmed to address different physics simultaneously. Partial differential equation (PDE) based FE modelling is a tool that can achieve this objective. Heat transfer, oxygen diffusion, and oxidation kinetics are different physical and chemical fields that concurrently exist in pavement ageing. The constitutive equations of these physical fields can be represented as ordinary differential equations (ODE) or PDE. As a general-purpose FE program, Comsol Multiphysics provides an efficient computational platform to solve PDEs. It can address the coupling effects of different physics, such as the viscoelastic asphalt mixture [27, 28] and the nonlinear elastoplastic aggregate base materials in the pavements [29].

To address the aforementioned research needs, this study develops a framework for modelling oxidative ageing of asphalt pavements from a multiphysics perspective. Specifically, a series of analytical models will be identified to quantify the influence of each physics on oxidative ageing. An equation-based approach will be employed to integrate these analytical models into the Comsol Multiphysics software. Subsequently, the integrated FE model will be used to simultaneously compute the change of each physics during oxidative ageing. The computational results will facilitate an understanding of the oxidative ageing mechanism of asphalt pavements. Finally, a database of physiochemical properties of field-oxidised asphalts will be collected from the existing literature. Model validation will be accomplished by comparing simulation results with field measurements in terms of the ageing product (the carbonyl area) of bitumen at different ageing times and pavement depths.

2 Analytical Models for Multiphysics Oxidative Ageing

Oxidative ageing of asphalt pavements is a complex process governed by oxidation kinetics, oxygen diffusion, and heat transfer.

2.1 Oxidative Kinetics Model

Oxidative kinetics of bitumen is characterised by the formation of carbonyl (C=O) and quantified by the carbonyl area (CA) measured from FTIR results. Jin et al. (2011) developed a two-reaction kinetics model to predict the reaction rate of CA in bitumen [10], as shown in **Equation 1.**

$$CA = CA_{tank} + (CA_o - CA_{tank})(1 - exp(-k_f t)\,) + k_c t \quad (1)$$

where CA_{tank} is the CA of the unaged tank bitumen; CA_o is the intercept of the constant-rate line, which is a unitless value; k_f and k_c are fast-rate and constant-rate reaction constants, respectively, in 1/day; and t is field ageing time. The fast and constant rate reaction constants k_f and k_c are temperature and binder-source dependent and can be predicted using the Arrhenius expression shown in **Equations 2 and 3.**

$$k_f = A_f\, e^{-E_{af}/RT} \quad (2)$$

$$k_c = A_c\, e^{-E_{ac}/RT} \quad (3)$$

where A_f and A_c are fast-rate and constant-rate pre-exponential factors, respectively, in 1/day, E_{af} and E_{ac} are fast-rate and constant-rate activation energies, respectively, in kJ/mol; R is the universal gas constant (R = 8.314 J/(mol·K)); and T is the absolute temperature, in K. To consider the oxygen partial pressure (as a measure of oxygen content), **Equations 2 and 3** were expanded to **Equations 4 and 5** [17].

$$k_f = A_f\, P^{\alpha} e^{-E_{af}/RT} \quad (4)$$

$$k_c = A_c P^{\alpha} e^{-E_{ac}/RT} \quad (5)$$

where P is the oxygen partial pressure and α is the reaction order for oxygen pressure. The terms $A_f\, P^{\alpha}$ and $A_c P^{\alpha}$ are described in ln(1/day) units.

2.2 Oxygen Transport Model

The oxygen transported in a pavement structure can be represented by the rate of oxygen pressure with time at any location within the asphalt layer. The oxygen transport model is shown in **Equation 6**, which is a 2nd order PDE [19]. The more aged the bitumen is, the more oxygen has been consumed; thus, the lower oxygen pressure will be in the transport media. Therefore, the equation uses the CA growth rate to quantify the oxygen consumption rate as a reducing factor to the oxygen transport process.

$$\frac{\partial P}{\partial t} = \nabla(fcf.Do\,\nabla P) - \frac{c_o\, T\, R}{h}.\frac{\partial CA}{\partial t} \quad (6)$$

$$h = h_o(1 + 0.0215\,(T - 30)) \quad (7)$$

where P is the oxygen pressure; ∇ is the location derivative $[\frac{d}{dx}, \frac{d}{dy}]$; D_o is oxygen diffusivity in pure bitumen in m^2/s; c_o is a factor that converts reaction rate of CA to rate of oxygen consumption (3.71×10^{-4} mol/ml); fcf is the field calibration factor and a calibration factor for the effect of fine matter in the mastic; and h is the solubility constant of oxygen in asphalt, which is a unitless value. Solubility is a temperature-sensitive parameter and can be altered for any temperature by using **Equation 7**, where h_o is the oxygen solubility in bitumen at a standard temperature of 30 °C ($h_o = 0.0076$) [30]. The oxygen diffusion coefficient is a function of the temperature and the viscosity of bitumen, as shown in **Equation 8** [31].

$$\frac{Do}{T} = 5.21 \times 10^{-12} LSV^{-0.55} \quad (8)$$

$$LSV = e^{(m+HS.CA)} \quad (9)$$

where LSV is the low-shear-rate-limiting viscosity (Pa.s), which is a measurement of the rheological properties of the asphalt binder when it is undisturbed by external forces [31]. LSV is temperature- and CA-dependent. HS is the asphalt hardening susceptibility (ln[Pa.s]/CA) which is the change in log-viscosity with respect to the change in CA, and m is an experimental parameter, which is the intercept of log-viscosity. HS and m are functions of temperature [31].

2.3 Heat Transfer Model

Fourier's law of heat conduction is used to determine the temperature profile across pavement depth, as shown in **Equation 10**. The thermal diffusivity of each pavement layer and the temperature transfer rate at the bottom of the pavement are specified in **Equations 11 and 12** [19].

$$\frac{\partial T}{\partial t} = \alpha \left(\frac{\partial^2 T}{\partial^2 y}\right) \quad (10)$$

$$\alpha = \frac{k}{\rho \,.c_p} \quad (11)$$

$$\frac{\partial T}{\partial y}\Big|_{3m} = constant \quad (12)$$

where y is the pavement depth, in meters; k is the thermal conductivity of the pavement layer, in W/(m. K); ρ is the corresponding material density, in kg/m^3; α is the heat diffusivity; and c_p is the heat capacity in J/(kg. K). This study assumed that temperature is constant at pavement depths below 3 meters. Moreover, a surface boundary for the heat transfer model was defined by Han et al. (2011) [19], which is represented by **Equation 13**.

$$\rho\, c_p \frac{\Delta y}{2} \frac{\partial T_s}{\partial t} = Q_s - \breve{\alpha}.\, Q_s + Q_a - Q_r - Q_c - Q_f \quad (13)$$

where T_s is the pavement surface temperature, in K; y is the pavement depth; Q_s is the heat flux due to solar radiation; $\breve{\alpha}$ is the albedo of the pavement surface (the fraction of reflected solar radiation); Q_a is the down-welling long-wave radiation heat flux from the atmosphere; Q_r is the outgoing long-wave radiation heat flux from the pavement surface; Q_c is the convective heat flux; and Q_f is the heat conduction from the surface into the pavement; with all heat fluxes expressed in W/m^2 [17].

3 Development of the Equation-Based Finite Element Model

The comprehensive oxidative ageing model was developed using Comsol Multiphysics software which consists of several components, including: (1) model geometry, (2) model interfaces, (3) model variables, (4) model parameters, (5) interpolation functions, and (6) user-defined materials properties. Details of each component are listed as follows.

3.1 Model Geometry

A two-dimensional geometry was developed in this study (**Figure 1**). The dimensions of the geometry are customised according to pavement structure and volumetric properties of the asphalt mixture. The geometry consists of three main domains: (1) interconnected air channels in the asphalt concrete (AC) layer, (2) mastic coating film and, (3) underlying pavement layers (base, subbase and subgrade). Herein, the thickness of the mastic coating film is defined as the diffusion depth (d_D) which is different from the conventional film thickness, in that it is the bitumen mastic coating film thickness that surrounds the interconnected air channels, not the aggregate particles [31]. **Figure 2** illustrates the idea of diffusion depth, where oxygen diffuses horizontally in a hollow cylinder from the air channel along the mastic coating thickness towards the mastic-aggregate interface. The diffusion depth ap-

proach is more realistic in reflecting the nature of the pavement structure in that the diffusion of oxygen into the mastic occurs via the surface area of the mastic exposed to air (i.e., surrounding air channels), rather than that surrounding the aggregate particles. The diffusion depth is defined in **Equation 14** [31].

$$d_D = \frac{V_{be}}{S_{ea}} \tag{14}$$

where V_{be} is the volume of effective binder (total volume of bitumen in the mix excluding the volume absorbed by aggregate), and S_{ea} is the exposed surface area of binder to the accessible air voids.

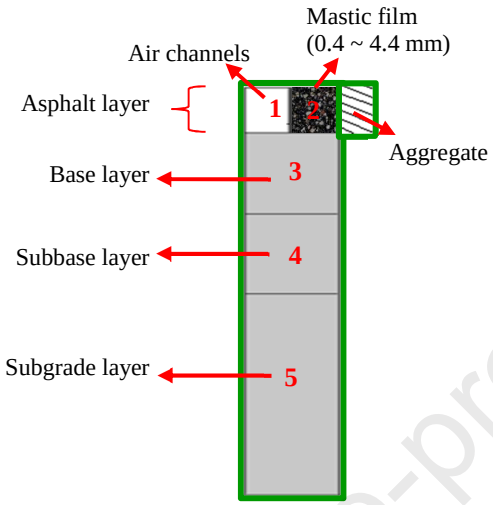

Fig. 1 Geometry of the integrated ageing model (not plotted to a scale). The domains of the geometry are identified by numbers (domain 1: interconnected air channels, domain 2: mastic coating film, domain 3: base layer, domain 4: subbase layer, and domain 5: subgrade layer). Domain 2 has two vertical interfaces, air-mastic interface and mastic-aggregate interface. Aggregate is not included in the geometry.

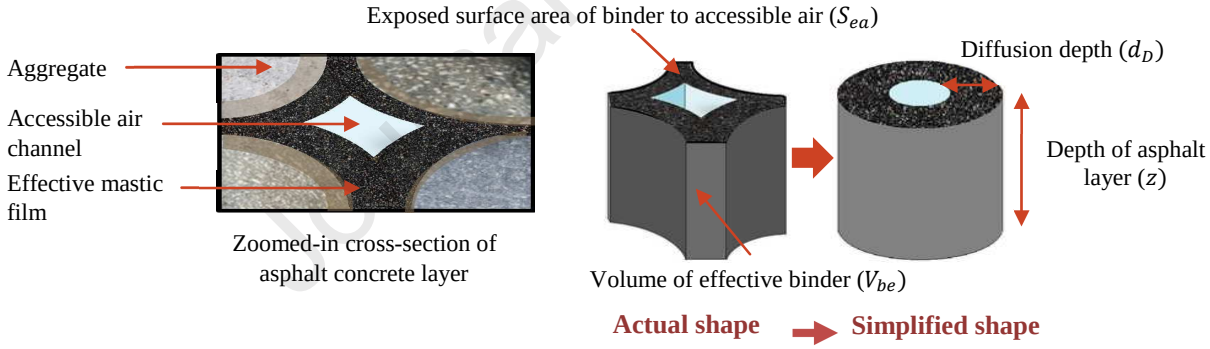

Fig. 2 Graphic illustration of the diffusion depth of oxygen in the asphalt pavement

The heat transition rate between the different pavement layers affects the temperature profile in the topmost layer (AC layer); consequently, it affects the overall oxidative ageing process in asphalt. Therefore, to accurately simulate the heat transfer, the proposed geometry includes the entire pavement structure even though underlying layers (i.e., base, subbase and subgrade layers) do not suffer from oxidative ageing.

3.2 Model Interfaces

This subsection describes the model interfaces to couple the analytical models discussed earlier into one integrated multiphysics ageing model.

3.2.1 Heat Transfer in Solids Interface

The time-dependent pavement temperature profile uses the Heat Transfer in Solids interface. This interface is commonly utilised to model the heat transfer in solids by conduction, convection and radiation, which can be used conveniently to simulate the pavement heat transfer processes. The basic equation defined by the software Comsol Multiphysics corresponds to the differential form of Fourier's law (illustrated in **Equation 10**) with some added customised inputs (i.e., heat sources) [28]. The general form of the equation is defined by:

$$\rho c_p \frac{\partial T}{\partial t} + \rho c_p u.\nabla T + \nabla.q = Q \quad (15)$$

$$q = -k\,\nabla T \quad (16)$$

where u is the velocity field defined by the transportation motion sub-node if parts of the model are moving in the material frame, and Q is the heat source (or sink) measured in W/m^3. The density ρ, heat capacity c_p, and thermal conductivity k are introduced to the model. Since the heat transfer interface is held active for all the domains in the geometry, therefore, the thermal properties for each domain are described in material components (**Section 3.4**).

The initial temperature in the geometry (at $t = 0$) is set to be the mean annual subsurface soil temperature which is measured at a depth of three meters [30]. The initial temperature was found to have negligible short-term effects on the heat transfer model and no impact on the overall ageing model.

The temperature at the lower boundary is considered a constant equal to the mean annual subsurface soil temperature. Therefore, the bottom boundary for the heat transfer interface depends on the climatic region where the road section is located. This assumption provides more area-specific inputs that can increase the accuracy of the temperature profile. The subsurface soil temperatures at different depths are available in the Climate Tool at the Long-Term Pavement Performance (LTPP) database. They are originally collected from the National Aeronautics and Space Administration (NASA), for the project Modern-Era Retrospective analysis for Research and Applications, Version 2 (MERRA-2), where the depths of the subsurface temperatures are available in detail.

The external vertical boundaries of the overall geometry are considered thermally insulated (no heat flux across the vertical borders); thus, the temperature gradient across the boundary is zero. The topmost boundary of the pavement (which makes up the upper borders for the air voids and mastic domains) is defined according to Han et al. (2011) in **Equation 13** [19]. This equation is broken down in the current model into several general inward heat flux equations. The convective heat flux is defined in the model using the equation:

$$Q_c = (T_{air} - T)\,h_c \quad (17)$$

where T_{air} is the air temperature at the road section, in K; and h_c is the heat transfer coefficient obtained by Vehrencamp's empirical equation (**Equation 18**) and employed by Lytton et al. (1993) and Han et al. (2011) for the determination of pavement temperature profiles by using the finite difference method [18, 19, 32].

$$h_c = 698.24 * 1.4\,(0.00144\left(abs\left(\frac{T+T_{air}}{2}\right)\right)^{0.3} * U_{wind}^{0.5} + 9.7 * 10^{-4} * \left(abs(T - T_{air})\right)^{0.3}) \quad (18)$$

where U_{wind} is the wind speed above the road section, in m/s. T_{air} and U_{wind} are hourly inputs, therefore they are introduced to the model as interpolation functions (refer to **Section 3.3.3**).

The down-welling and ongoing long-wave radiations are defined as:

$$Q_a - Q_c = 5.67 * 10^{-8} * (ac * {T_{air}}^4 - ec * T^4) \quad (19)$$

where ac is the absorption coefficient of the pavement, which is described in **Section 3.3.2** as a model parameter which depends on the climatic region, and ec is the emission coefficient of the pavement, which is a time-dependent coefficient; therefore, it is introduced in **Section 3.3.3** using an interpolation function.

Finally, the heat flux within the pavement at the surface is expressed by Fourier's law:

$$Q_f = -k\frac{\partial T}{\partial x} \quad (20)$$

The heat transfer physics employs the LTPP Climate Tool to obtain the site-specific hourly air temperature, wind speed, solar radiation, albedo and the emissivity values. Therefore, this model covers more time-dependent parameters, such as albedo and emissivity coefficient, which were considered constants or seasonal variables in the previous pavement profile prediction model [33]. Additionally, the previous model calculated the hourly heat flux on the surface, and then calculated the temperature profile at different depths by using the finite-difference approximation. In contrast, this model measures the temperature profile at any point simultaneously. Another improvement is that the current model uses the field mean subsurface soil temperature as a bottom boundary, which is location-dependent and more reasonable, rather than using a fixed decline rate or a constant value for all the climatic regions.

3.2.2 Coefficient Form Partial Differential Equation Interface – Oxygen Diffusion in the Interconnected Air Channels (Vertical Diffusion)

Oxygen diffuses from the ambient air into the interconnected air channels first, before it spreads into the bitumen mass. Therefore, it is imperative to simulate oxygen diffusion from the air to the accessible air channels. The weak

form interface and the coefficient form PDE interface can be used to simulate oxygen diffusion in the air voids; the latter is detailed here. The coefficient form PDE interface is a general interface that can solve one dependent variable in up to second-order derivatives in both time and space [28]. The general form of the equation is:

$$\frac{\partial^2 u}{\partial t^2} + d_a \frac{\partial u}{\partial t} + \nabla.(-c\,\nabla u - \propto u + \gamma) + \beta.\nabla u + au = f \quad (21)$$

$$\nabla = [\frac{\partial}{\partial x}, \frac{\partial}{\partial y}] \quad (22)$$

where u is the dependent variable to solve for, and d_a, c, γ, β, a and f are user-defined coefficients. To utilise the general form PDE in **Equation 21** to determine oxygen diffusion in the interconnected air channels as expressed in **Equation 6**: u is defined as the partial pressure of oxygen (P_{air}); c is defined as the coefficient of oxygen diffusion in the air voids (D_{o_2}) which is related to the air voids percentage in the AC mix; γ, β, and a are all substituted by zero; and d_a is replaced by 1. The source term f is expressed by:

$$f = -\frac{c_o RT}{h} . \frac{\partial CA}{\partial t} \quad (23)$$

This interface is held active for the interconnected air channels domain only (domain 1 in **Figure 1**). The amount of oxygen in the AC matrix is measured and represented by the oxygen partial pressure, as described in **Equation 6**. According to **Equation 6**, the oxygen consumption rate is inversely proportional to the CA-growth rate. The same also applies to the oxygen content in the air channels; therefore, the carbonyl area considered in this physics is CA at the air channel-mastic interface, namely, CA_i. The approximate diffusion coefficient (D_{o_2}) in the air channels is obtained from the work of Wen and Wang (2018) by correlating D_{O2} to the air voids content in the asphalt mixture [34]. Therefore, D_{o_2} is a constant that is dependent on the asphalt morphology. Moreover, the field correction factor fcf mentioned in **Equation 6** is given a value of 1 for the diffusion of oxygen in the air channels.

The initial value for the oxygen partial pressure is considered equal to the oxygen pressure in the ambient air (0.2 atm), while the initial oxygen partial pressure rate (at $t = 0$) is zero. Additionally, since the air channel is connected to the atmospheric air, the boundary condition of the oxygen partial pressure at the topmost surface of the air voids channel is taken to be 0.2 atm at any time. The same applies to the AC-base course interface, where the unbound base layer is assumed to be porous, thus allowing free access of the air to the AC layer [21]. Therefore, oxygen partial pressure at the bottom surface boundary of the air voids channels (domain 1 in **Figure 1**) equals 0.2 atm [33]. When a treated base is used, such as cement or asphalt treated base, access to free air is constrained, leading to the unavailability of oxygen; thus, the oxygen partial pressure at any time will be zero. One additional BC is considered here: the interface between the air channel and the bitumen coating surface (bounds domain 1 from the right side in **Figure 1**). The partial pressure here is interchangeable (circularly dependent) between the air-channels and the mastic coating. Therefore, the boundary condition is defined as ($P_{air} = P_b$), where P_b is the oxygen partial pressure in the AC mastic.

3.2.3 Coefficient Form Partial Differential Equation Interface – Oxygen Diffusion Inside the Mastic Coating Film (Horizontal Diffusion)

When oxygen diffuses into the interconnected air channels, it then spreads into the bitumen mastic and causes oxidation. The coefficient form PDE interface (expressed in **Equation 21**) is utilised to simulate the diffusion process of oxygen in the mastic phase. Therefore, the interface is activated in domain 2 (shown in **Figure 1**), which represents the AC mastic coating film. In this interface, the oxygen partial pressure (P_b) describes the oxygen content by using **Equation 6**. However, c is replaced here by a CA- and temperature-dependent variable (D_o) according to **Equation 8,** unlike the coefficient of oxygen diffusion in the air channels (D_{o2}) which was a constant value and dependent on the structure of the mixture (air voids content-dependent). Since D_o is not constant, it is introduced to the model as a variable (**Section 3.3.1**). Additionally, since oxygen diffusion is carbonyl area dependent (**Equation 6**), the carbonyl area considered here is the stationary carbonyl area inside the mastic film (domain 2 in **Figure 1**), namely (CA_b). Whereas the field calibration factor fcf was given a value of 1 because all the AC volumetric properties are available.

The boundary conditions of this interface are defined as follows. The initial partial oxygen pressure is considered to have a small initial value of 0.0001 atm, and the initial rate of oxygen partial pressure is set to zero. Since the topmost and bottom surfaces of mastic are freely exposed to the ambient atmospheric air, the oxygen partial pressure at these two BCs is defined as 0.2 atm at any time. The BC at the mastic-air channels interface (shown in **Figure 1** as a vertical line between domains 1 and 2) is defined as ($P_b = P_{air}$). Therefore, this interface is circularly dependent on the vertical diffusion of oxygen in the air channels interface. In other words, the oxygen partial pressure in the air channels model serves as a line BC for the oxygen partial pressure in the mastic interface.

Oxygen diffusion within the asphalt layer is a central component of modelling the oxidation process. However, the rate and extent of oxidation are bitumen-source dependent; therefore, the following two model interfaces are employed to simulate oxidation kinetics. Two different interfaces for the oxidation rate are necessary because it is also oxygen pressure dependent. Furthermore, since the air channels possess a coefficient of oxygen diffusion different from that in the bitumen mastic, an interface is needed to simulate the carbonyl growth at the mastic-air channel interface and use it as a boundary condition for the growth of carbonyl inside the mastic.

3.2.4 Coefficient Form Partial Differential Equation Interface – Carbonyl Area at the Mastic-air Channels Interface

This interface is held active at domain 1 (shown in **Figure 1**) to determine the growth of carbonyl at the mastic-air channels interface. The model uses the differential form of **Equation 1**, shown in **Equation 24** [17] to predict the carbonyl area (CA_i).

$$\frac{\partial CA_i}{\partial t} = M_{RTFO} k_f e^{-k_f t} + k_c \tag{24}$$

where M_{RTFO} is the limiting amount of carbonyl formation due to the first-order reaction after hot mix production. It can be obtained by plotting the carbonyl growth rate for the short-term and long-term laboratory aged bitumen. To utilise the general form PDE in **Equation 21** to determine the carbonyl area at any time at the mastic-air interface as in **Equation 24**: u (in **Equation 21)** is defined as the carbonyl area at the mastic-air channels face (CA_i); c, γ, β, and a are all substituted by zero, and d_a is replaced by 1. The source term f is expressed by:

$$f = M_{RTFO} k_f e^{-k_f t} + k_c \tag{25}$$

The initial value for CA_i can be obtained by conducting an FTIR scanning test for the unaged bitumen binder, and the initial carbonyl rate (at $t = 0$) is defined to be zero. The carbonyl area CA_i at the BC where the air channels and mastic meet is made equal to CA in the mastic domain (CA_b) so that the two domains will have circular dependency (i.e., $CA_i = CA_b$ at the BC).

3.2.5 Coefficient Form Partial Differential Equation Interface – Carbonyl Area in the Asphalt Mastic

The coefficient form PDE interface is employed to simulate the oxidation kinetics inside the mastic (domain 2 shown in **Figure 1**). The model uses **Equation 24** to predict the growth of CA in the mastic domain. Similar to **Equation 24** that is being used to simulate the carbonyl growth at the mastic-air channels interface, **Equation 26** is implemented to predict the growth of carbonyl functional groups in the mastic CA_b (domain 2 in **Figure 1**).

$$\frac{\partial CA_b}{\partial t} = M_{RTFO} k_f e^{-k_f t} + k_c \tag{26}$$

The initial value (at $t = 0$) is set to be the carbonyl area in the virgin (unaged) bitumen. The bitumen-air channels interface (domain 1- domain 2 interface) is defined as ($CA_b = CA_i$) to allow the circular-dependency between the two carbonyl interfaces.

3.3 Model Variables, Parameters and Time-dependent Parameter

3.3.1 Model Variables

The following variables are defined:

1- Heat transfer coefficient (h_c), as defined in **Equation 19**. The equation is written in the following format:

$$h_c = 697.33 * (0.000144 * (if(((T/1[K] + T_{air}(t)/1[K])/2) == 0, abs(((T/1[K] + T_{air}(t)/1[K])/2) + 0.00001), abs((T/1[K] + T_{air}(t)/1[K])/2)))\text{^}0.3 * (U_{wind}(t)/1[m/s])\text{^}0.7 + 0.00097 * (if(((T/1[K] - 273.15) - (T_{air}(t)/1[K] - 273.15)) == 0, abs(0.00001 + ((T/1[K] - 273.15) - (T_{air}(t)/1[K] - 273.15))), abs(((T/1[K] - 273.15) - (T_{air}(t)/1[K] - 273.15)))))\text{^}0.3) \tag{27}$$

2- Oxidation kinetics coefficients (k_f and k_c), as defined in **Equations 4 and 5**. Since k_f and k_c are oxygen pressure-dependent; they are defined separately for the air-channels (domain 1) and mastic (domain 2) as follows:

In the air channels:

$$k_f = A_f * (P_{air}/101325[Pa])\text{^}\alpha * exp(-E_{af}/R/T) \tag{28}$$

$$k_c = A_c * (P_{air}/101325[Pa])\text{^}\alpha * exp(-E_{ac}/R/T) \tag{29}$$

In the mastic:

$$k_f = A_f * (P_b/101325[Pa])\text{^}\alpha * exp(-E_{af}/R/T) \tag{30}$$

$$k_c = A_c * (P_b/101325[Pa])\text{^}\alpha * exp(-E_{ac}/R/T) \tag{31}$$

3- Diffusion of oxygen in the bitumen coefficient (D_o), as defined in **Equation 8** and written in the following format:

$$D_o = ((5.21E-12) * (LSV\text{^} - 0.55) * T)/1[K * s/m\text{^}2] \quad (32)$$

4- Low shear rate-limiting viscosity (LSV), as defined in **Equation 9** and written in the following format:

$$LSV = exp(m + HS * CA_b) \quad (33)$$

5- Coefficient of oxygen solubility in the bitumen (h), as defined in **Equation 7** and written in the following format:

$$h = h_o * (1 + 0.0215 * (T/1[K] - 273.15 - 30)) \quad (34)$$

3.3.2 Model Parameters

The model parameters include:

1. Geometry dimensions (obtained from the structural design specifications of the pavement and the volumetric characteristics of the AC mix).
2. Oxidation kinetics constants M_{RTFO},CA_o, A_c, A_f, HS, E_{af}, E_{ac}, and m. These parameters can be obtained by performing laboratory ageing tests (rolling thin film oven and pressurised ageing vessel tests), rheological tests, and FTIR to obtain CA at different ageing stages [31].
3. The oxygen diffusion coefficient in the air voids channels (D_{o2}). It can be obtained from the empirical measurements provided by Wen and Wang (2018) by determining the air voids percentage from the mixture volumetric properties [34].
4. The temperature at the bottom of the pavement and the initial temperature (at $t = 0$). These temperatures are considered equal to the subsurface soil temperature at a depth of 3 meters, which is available in the LTPP Climate Tool database for various regions.
5. The field correction factor, fcf, which is utilised to correct the coefficient of oxygen diffusion in the mastic in case there is not enough information about the binder absorbed by the aggregate and the existence of fine matter in the mastic.

3.3.3 Interpolation Functions

The interpolation functions are the time-dependent inputs. They are introduced into the Comsol program by tables or files containing the functions in discrete points [28]. Therefore, they can be generated to introduce the time-dependent climate inputs needed for the pavement temperature model. These inputs include the hourly records of shortwave solar radiation, air temperature, wind speed, emissivity, and albedo values. These hourly climate data can be obtained from the LTPP Climate Tool for different climatic regions.

3.4 Material Properties

Heat transfer in the pavement depends on the thermal properties of the pavement materials. Therefore, the thermal characteristics of the pavement layers are introduced to the model in this section. The inputs for each layer (for each domain in **Figure 1**) include thermal conductivity, density and heat capacity. The thermal properties of the air channels (domain 1) and the mastic coating film (domain 2) are similar as they both represent the AC layer in the heat transfer interface. The sensitivity and significance of each parameter on the pavement temperature prediction model were assessed in previous studies. It was found that the thermal diffusivity of AC, which is a term that combines thermal conductivity, density, and heat capacity (**Equation 35**), had negligible effects on model accuracy if it was kept in the range of 4.4 – 6.4 x 10^{-7} m^2/s [19, 35].

$$\kappa = \frac{k}{\rho . C_p} \quad (35)$$

Due to the lack of field measurements, the thermal properties of the pavement layers were collected from the literature [36-47], and the current study employed the mean values of those obtained from the literature. **Table 1** lists the thermal properties used for each pavement layer in this study. There is no evidence of significant changes to the thermal properties of asphalt pavement upon ageing [43]; therefore, the materials thermal properties are kept constant.

Table 1. Thermal properties of pavement layers used in this study

Pavement layer	Thermal conductivity, k (W/m.K)	Heat capacity, c_p (J/kg.K)	Density, ρ, (kg/m^3)
Asphalt concrete	2.3	960	2450
Base and sub-base	1.5	805	2350
Subgrade	1.7	1100	2200

4 Validation of the Pavement Temperature Model

The temperature profile of the pavement plays a vital role in the oxidative ageing process. When the temperature increases, the diffusivity of oxygen in the mastic increases, and oxidation accelerates, which subsequently leads to more oxidative ageing in the pavement. Similarly, when the temperature drops, the bitumen in the asphalt mixture will suffer from a temporary physical hardening (increase in viscosity), which blocks or decreases oxidation of the pavement, leading to a slower oxidative ageing rate. Therefore, it is crucial to ensure the accuracy of the predicted temperature profiles.

Since the time-dependent heat transfer interface is independent of the other physics of ageing, it can be run and validated individually before combining it into the integrated ageing model. The LTPP database contains the hourly field temperatures of 82 road sections in different climate regions across the United States. The field temperatures were collected using thermistors installed at different pavement depths, and the collected data are available for specified time intervals.

This study selected three road sections from different climate regions, including (1) road section 48-1068 in Lamar, Texas, USA (in wet, no freeze region); (2) road section 27-1028 in Otter Tail, Minnesota, USA (in wet, freeze region); and (3) road section 16-1010 in Idaho, USA (in dry, freeze region). **Figure 3** shows the location of the selected sections, and **Table 2** contains the structures of the road sections. The predicted pavement temperature profiles were compared against the hourly recorded temperatures from five thermistors installed at different pavement depths. **Table 3** lists the depths of the thermistor locations measured from the surface of the pavement for road sections 48-1068, 27-1028 and 16-1010.

Fig. 3 Distribution map for the selected road sections to predict the pavement temperature profiles

Table 2. Pavement structures of identified LTPP sections

Layer description	Layer code	Layer type	Representative thickness (mm)
Road section 48 – 1068 in Lamar, Texas			
Asphalt overlay	AC	asphalt concrete layer	80
Original asphalt layer	AC	asphalt concrete layer	198
Base layer	GB	unbound (granular) base	152
Subbase layer	TS	bound (treated) subbase	203
Subgrade	SS	subgrade (untreated)	N/A
Road section 27- 1028 in Otter Tail, Minnesota			

Asphalt overlay	AC	asphalt concrete layer	41
Original AC layer	AC	asphalt concrete layer	51
AC treated base layer	AC	asphalt concrete layer	152
Subgrade	SS	subgrade (untreated)	N/A
Road section 16-1010 in Idaho			
Asphalt overlay	AC	asphalt concrete layer	132
Original AC layer	AC	asphalt concrete layer	145
Base layer	GB	unbound (granular base)	137
Subgrade	SS	subgrade (untreated)	N/A

Table 3. Location of thermistors for identified LTPP sections

Thermistor identification number	Depth from the pavement surface (m)
Road Section 48-1068 in Lamar, Texas	
1	0.025
2	0.128
3	0.232
4	0.321
5	0.397
Road Section 27-1028 in Otter Tail, Minnesota	
1	0.025
2	0.115
3	0.205
4	0.623
5	0.696
Road Section 16-1010 in Idaho	
1	0.023
2	0.13
3	0.25
4	0.34
5	0.42

In addition to the pavement structure, the hourly air temperatures, wind speed, short-wave solar radiation, albedo, and emissivity were collected from the LTPP database and incorporated into the temperature prediction models. Optimised absorption coefficients were employed by region. For road sections 48-1086, 27-1028, and 16-1010, Han et al. (2011) proposed the following absorption coefficients: 0.7, 0.75, and 0.7, respectively [19]. The mean subsurface soil temperatures obtained from MERRA-2 were 17, 5.3 and 6.3°C for road sections 48-1068, 27-1028, and 16-1010, respectively. These subsurface soil temperatures were considered the bottom boundary condition for the temperature prediction models. Previous studies regarded temperature as a constant value (33.5 ºC) or changing at a constant rate for depths below three meters [19]. Therefore, using actual site-specific soil temperatures is expected to provide greater accuracy, especially for deeper pavement layers.

Figures 4, **5,** and **6** compare predicted hourly pavement temperatures with field-measured temperatures at different pavement depths over time for road sections 48-1068, 27-1028 and 16-1010, respectively. These figures show that predicted temperatures at various pavement depths are comparable to those measured in the field. Daily temperature variations are reduced as pavement depth increases. For validation purposes, the models were run for a minimum of one year to capture the temperature prediction in all seasons. The time interval is also bounded by the availability of field measurements in the LTPP database. The mean absolute error (MAE) is measured at five pavement depths for each road section and detailed in **Figures 4-6**.

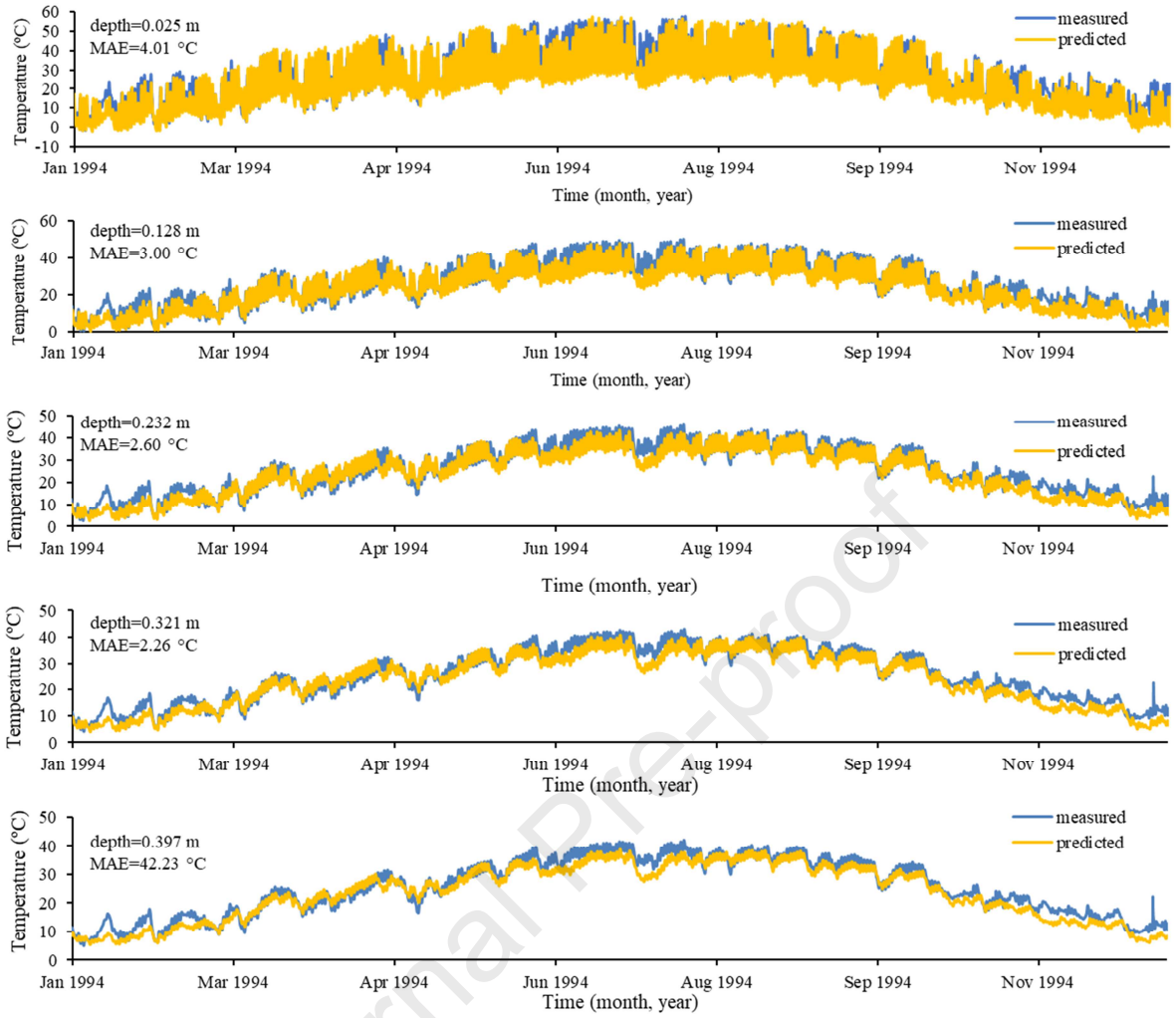

Fig. 4 Predicted and field-measured temperatures for road section 48-1068 in Lamar, Texas, USA, for one year (January 1994-December 1994) at depths of 0.025, 0.128, 0.232, 0.321, and 0.397 m, respectively, measured from the surface of the pavement with the mean absolute error (MAE) at different depths.

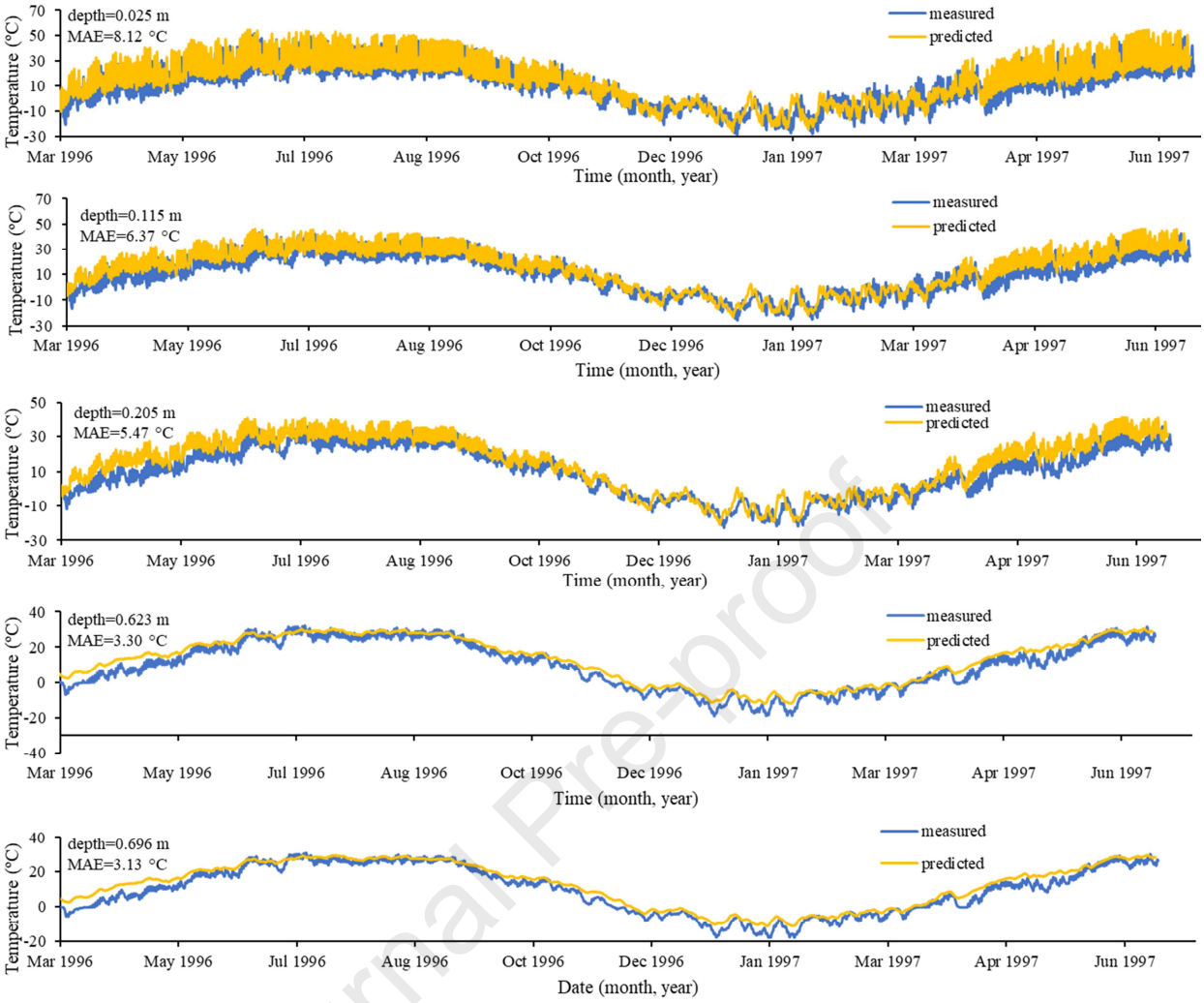

Fig. 5 Predicted and field-measured temperatures for road section 27-1028 in Otter Tail, Minnesota, USA, for the time period (March 1996-June 1997) at depths of 0.025, 0.115, 0.205, 0.623, and 0.696 m, respectively, measured from the surface of the pavement with the mean absolute error (MAE) at different depths.

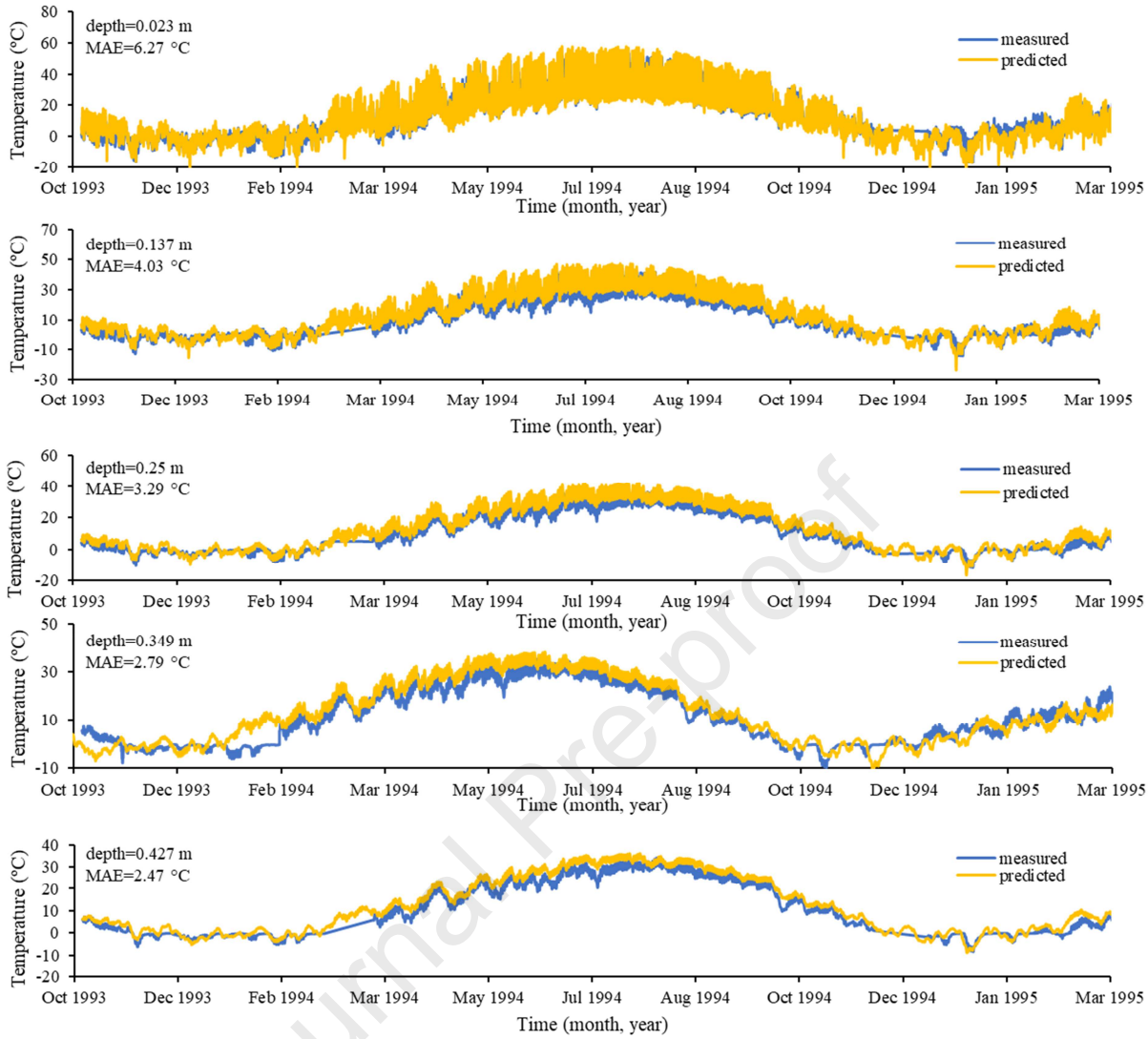

Fig. 6 Predicted and field temperatures for road section 16-1010 in Idaho, USA, for the time period (October 1993-March 1995) at depths of 0.023, 0.137, 0.25, 0.349, and 0.427 m, respectively, measured from the surface of the pavement with the mean absolute error (MAE) at different depths.

The maximum mean absolute error (MAE) values of 8.12 ºC and 6.27 ºC were encountered close to the pavement surface at 0.025 m and 0.023 m in the cold (freeze) regions (Minnesota and Idaho), and the error was more distinct in the winter season. Thus, the error was likely caused by using empirical parameters for the heat transfer equation, specifically the heat conduction coefficient between the pavement surface and the air (h_c). These parameters were obtained by experimental tests under ideal conditions where the surface temperature is always higher than the air temperature with a variance range of 6.3 to 26 ºC [32]. Field conditions do not always match this assumption. For example, in regions susceptible to freezing, the air temperature is higher than pavement temperature during the winter season. This causes heat to transfer from the air to the pavement, not the opposite direction (pavement to air). Physically, the heat conduction rate is assumed to be the same regardless of the route of heat transfer (air to/from pavement surface); however, there are no data to support this assumption. Nonetheless, the model appears to have sufficient accuracy, particularly for ageing prediction purposes where ageing occurs at high temperatures and stops when the temperature is low, which suggests that the small divergence during cold seasons will not affect oxidative ageing.

Using the empirical equation proposed by Vehrencamp (**Equation 17**)[32] in freezing conditions causes the heat transfer coefficient due to conduction (h_c) to drop, which creates a divergence between predicted and measured temperatures during the winter season (shown in **Figure 7**) and causes an MAE of more than 12 ºC. Therefore, a limitation is proposed for the heat conduction equation so that if the difference in temperature between the air and pavement surface exceeds -4 ºC, it will not cause the heat conduction to drop radically (as shown in **Equa-**

tion 36). This constraint is done to ensure a certain level of heat conduction is achieved even during the freezing condition, a condition which the empirical conduction equation (**Equation 17**) did not cover.

$$Q_c = (if\ (T_{air}(t) - T) > -4, -4,\ (T_{air} - T))\ h_c \quad (36)$$

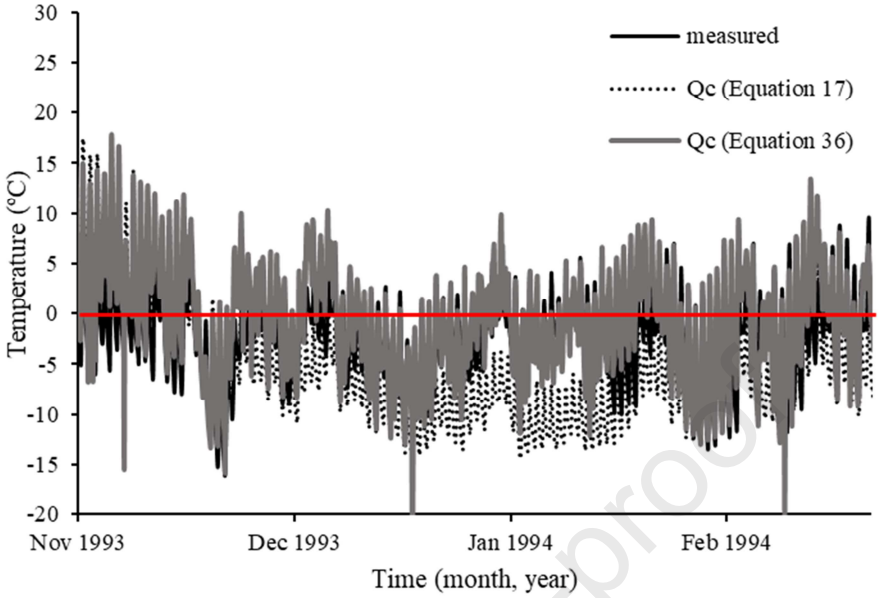

Fig. 7 Divergence between predicted and measured temperatures before and after applying a minimum limit to h_c

5 The Integrated Ageing Model

Two road sections were selected to run the integrated ageing model: US277 and US83, both located in Texas, USA. These sections were chosen in two different climate regions and due to the availability of the Carbonyl Area (CA) values in the binder at different ageing periods, which will be used to validate model predictions. Ageing data were collected from the Federal Highway Administration (FHWA) reports [31]. In addition to CA, properties of binders, mixtures, and pavement structures were also recorded. Aged binders were extracted and recovered from field-aged cores that were sliced into several pieces with a thickness of 12.7 mm and then tested using FTIR to determine CA values [17, 31, 33]. **Table 4** shows general information of the mixture and binder types as well as the environmental zones for these sections [17, 31, 33]. **Table 5** lists the oxidation kinetics and viscosity hardening properties of the virgin binders. **Figure 8** illustrates the pavement structures for road sections US277 and US83 [48, 49].

In addition to setting up the geometry for the ageing models, the pavement structure is also employed to estimate the coefficient of oxygen diffusion in the air channels (D_{o2}). To do so, a set of experimental data comparing measured D_{o2} with accessible air voids (AAV) percentage ($D_{o2}\left(\frac{cm^2}{s}\right) = 3 \times 10^{-4} AAV\% - 14 \times 10^{-4}, R^2 = 0.6014$) was employed to form an estimation of the D_{o2} values [34]. Since AAV% is recorded in FHWA reports (**Table 4**), the coefficients of oxygen diffusion in the interconnected air channels for road sections US277 and US83 were calculated by regression to be 3.79 * 10^{-4} cm^3/s and 3.68 * 10^{-4} cm^3/s, respectively. Whereas, other volumetric properties such as the mean radius of air voids and diffusion depths were available for road sections US277 and US83 and employed as the thicknesses for air channel (thickness of domain 1 in **Figure 1**) and mastic film (thickness of domain 2 in **Figure 1**), respectively.

Other inputs for the model include hourly climate data (air temperatures, wind speed, shortwave solar radiation, albedo, and emissivity) obtained from the Climate Tool in the LTPP database. The ageing models can be run for any duration; however, for model validation purposes in the current study, the durations were limited according to the availability of field carbonyl data. Therefore, hourly climate data were collected for July 2008 - January 2012 for road section US277 when the last coring sample was extruded in January 2012. Whereas, for road section US83, hourly climate data were collected for July 2008 – November 2011. Since the selected road sections are located in different environmental regions, the absorption coefficients (ac) will differ. Absorption coefficients were obtained from the environmental parametric study conducted by Han (2011) [33], with values of 0.75 and 0.7 for road sections US277 and US83, respectively.

Table 4. General Information on mixture and binder types used for road sections US277 and US83 [17, 19, 31, 33]

Road Section - Location	Environmental zone	AC cores thickness (mm)	Binder supplier	PG (modifier)	AAV (%)	Construction date
US277 - Laredo, Texas	Dry-Warm	76.2	Valero-type C	70-22 (SBS)	7.27	2008
US83 - Childress, Texas	Dry-Cold	50.8	SEM-Type D	PG 70-28	7.7	06/ 2008

Table 5. Oxidation kinetics parameters for road sections US277 and US83 [17, 19, 31, 33]

Road	$A_c P^{\propto}$ (CA/Day)	$A_f P^{\propto}$ (CA/Day)	HS (1/CA)	m (ln(Pa.s))	CA_o	CA_{RTFO}	fcf	M_{RTFO}	E_{af} (kJ/mol)	E_{ac} (kJ/mol)
US277	3.26 $*10^{13}$	3.27 $*10^{10}$	3.970	5.84	0.826	0.740	1.2	0.05	75.4	103.8
US83	1.03 $*10^{9}$	3.34 $*10^{7}$	4.53	7.89	0.594	0.814	12	0.12	49.1	72.5

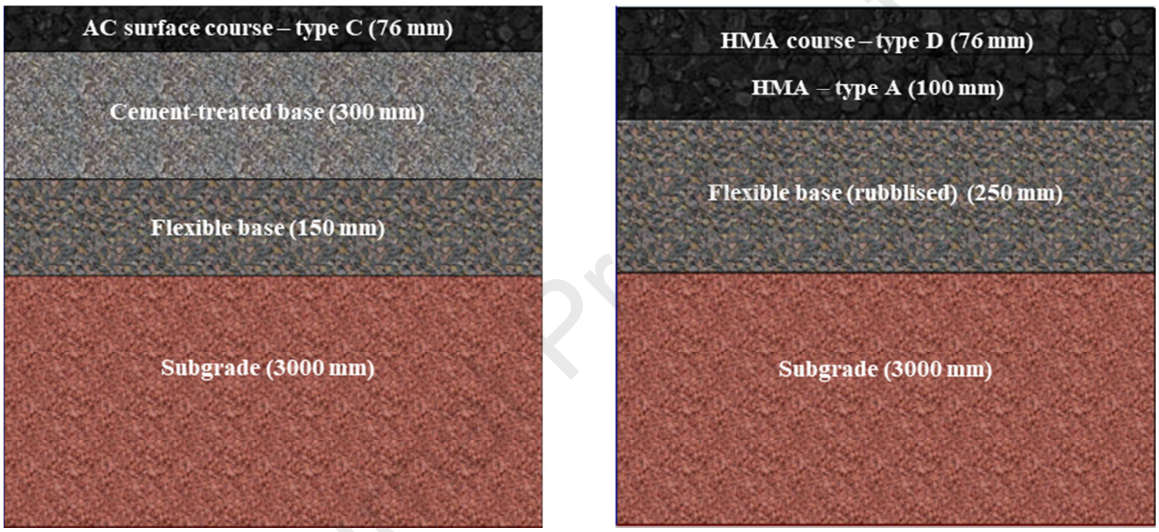

(a) **(b)**

Fig. 8 Pavement profiles of (a) Road section US277 in Laredo, Texas, USA; and (b) Road section US83 in Childress, Texas, USA.

6 Results

After developing the equation-based modelling framework for oxidative ageing of asphalt pavements and collecting all climatic data, binder properties, and pavement structure inputs, two pavement models were run. Data were collected for every one-hour interval, with outputs including the pavement temperature profile, partial oxygen pressure in the air channels, partial oxygen pressure inside the mastic, and the carbonyl area within the mastic.

6.1 Pavement Temperature Profile

The heat transfer in solids interface predicted pavement temperature at any depth across the pavement profile. Outputs for each hour at any location within the pavement structure were obtained and employed simultaneously in the other interfaces (i.e., oxygen diffusion and oxidation kinetics). The temperature profile is a one-way process which means it is not affected by the oxygen pressure distribution or the carbonyl area growth within the pavement structure; however, it plays a significant role on the pressure distribution and the growth rate of the oxidation products. **Figure 9** shows temperature change plotted against time for road section US277 at different depths of the AC layer and the temperature variation with AC depth at different time intervals. Since the topmost layers are closer to atmospheric seasonal changes, temperatures at the surface show more seasonal variation than those in deeper layers. Additionally, the daily temperature variation between daytime and nighttime is more pronounced at the pavement surface than at greater depths.

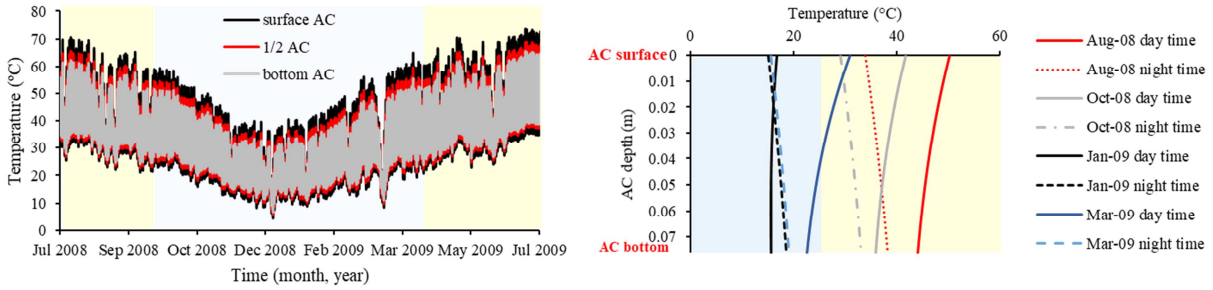

(a) (b)

Fig. 9 Temperature profile for road section US277, located in Laredo, Texas, USA. (a) Temperature plotted against time at three AC depths (surface, ½ AC, and bottom of AC layer) for a duration of one year. (b) Temperature profile for the AC layer at four different times throughout the year. Winter and summer seasons are highlighted with blue and yellow colours, respectively.

6.2 Partial Oxygen Pressure in the Interconnected Air Channels

The accessibility and distribution of oxygen within the pavement play a vital role in the rate of oxidative ageing of asphalt pavement. Without a continuous supply of oxygen from the surrounding atmosphere into interconnected air channels and then to the bitumen in the mastic film, the oxidation process will stop. The coefficient of oxygen diffusion in the air channels is a constant value that depends on the percentage of air voids, whereas the coefficient of oxygen diffusion in the mastic is a function of CA and temperature. While the coefficient of oxygen diffusion in the air channels is approximately 1000 times greater than that in the mastic, oxygen distribution in the air and the mastic are circularly linked. Oxygen in the air channels is supplied by the ambient atmosphere, and it will be consumed by the binder in the asphalt mastic due to oxidation; therefore, more oxygen will transport from the air into the air voids and then into the mastic.

Figure 10 shows the partial oxygen pressure distribution in the air channels (domain 1 in **Figure 1**) for road section US277 over a period of 3.5 years. As expected, the oxygen pressure varies between 0 – 0.2 atm, as the oxygen pressure in the atmosphere is 0.2 atm. The oxygen partial pressure is low with high daily variations during the summer season because the surrounding mastic consumes more oxygen in the oxidation process in summer. In contrast, the oxygen pressure is high with low daily variations in the winter because the oxidation rate is low in this season due to low temperatures. Similar patterns were observed for road section US83.

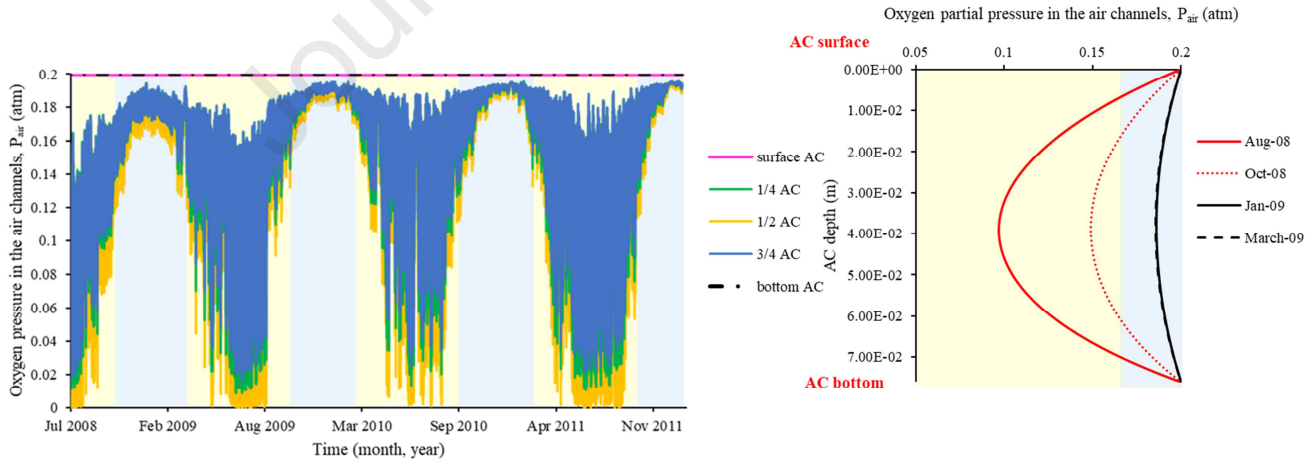

(a) (b)

Fig. 10 Oxygen partial pressure distribution in the air channels for road section US277, located in Laredo, Texas, USA. (a) Oxygen partial pressure in the air channels plotted against ageing time at different AC depths (surface, ¼ AC, ½ AC, ¾ AC, and bottom of AC layer). (b) Oxygen pressure in the air channels against depth of AC layer at different field ageing times. Winter and summer seasons are highlighted in blue and yellow colours, respectively.

In this model, oxygen can diffuse freely from the air into the interconnected air channels from both the topmost surface and the bottom of the asphalt layer, assuming the base material is crushed stones of high porosity. Therefore, complete access of oxygen into the pavement is assumed [33, 34]. Consequently, **Figures 10 (a)** and **(b)** show that the oxygen pressure in the middle of the AC layer (1/2 AC) is low and it becomes higher at the top and

bottom of the AC layer due to the boundary conditions; this forms a clear C-shaped curve across the pavement depth. This observation is consistent with the oxygen distribution in the field observed by Wang et al. (2014) [21].

Although the oxygen movement is two-dimensional, due to the *relatively* high diffusivity of oxygen in the air channels, there is no clear difference in the oxygen partial pressure in the horizontal direction (x-direction) within the air channels domain (domain 1 in **Figure 1**). However, there is a considerable difference in the vertical direction as oxygen was supplied from the top and bottom surfaces of the AC layer. For this reason, this interface is referred to as the *vertical* diffusion of oxygen in the interconnected air channels.

6.3 Partial Oxygen Pressure in the Asphalt Mastic

When exposed to oxygen and high temperatures, the bitumen in the asphalt mastic will suffer from oxidation. As a result, it will consume the oxygen that diffused into the mastic. When the temperature is low, the oxidation process will be halted as the energy required to initiate oxidation is not reached; therefore, the oxygen will not be consumed, and the oxygen pressure will increase in the mastic due to continuous oxygen diffusion in the mastic. **Figure 11** shows the oxygen pressure distribution in the asphalt mastic (labelled as domain 2 in **Figure 1**). **Figure 11 (a)** shows that the oxygen pressure in the mastic follows the same pattern as that in the air channels (**Figure 10**) but with lower oxygen pressures in the mastic. This is reasonable as the oxygen from the air diffuses through more steps to reach the mastic and oxygen is consumed by the oxidative reactions. As shown in **Figure 11 (b)**, the oxygen pressure in the mastic forms a C-shaped curve where the middle AC layer (1/2 AC) has low oxygen pressure, while the top and bottom surfaces of the AC layer have much higher oxygen pressures as they are exposed to atmospheric air pressure. The oxygen pressure in winter is consistently higher than in summer as oxygen is consumed due to severe oxidation in summer.

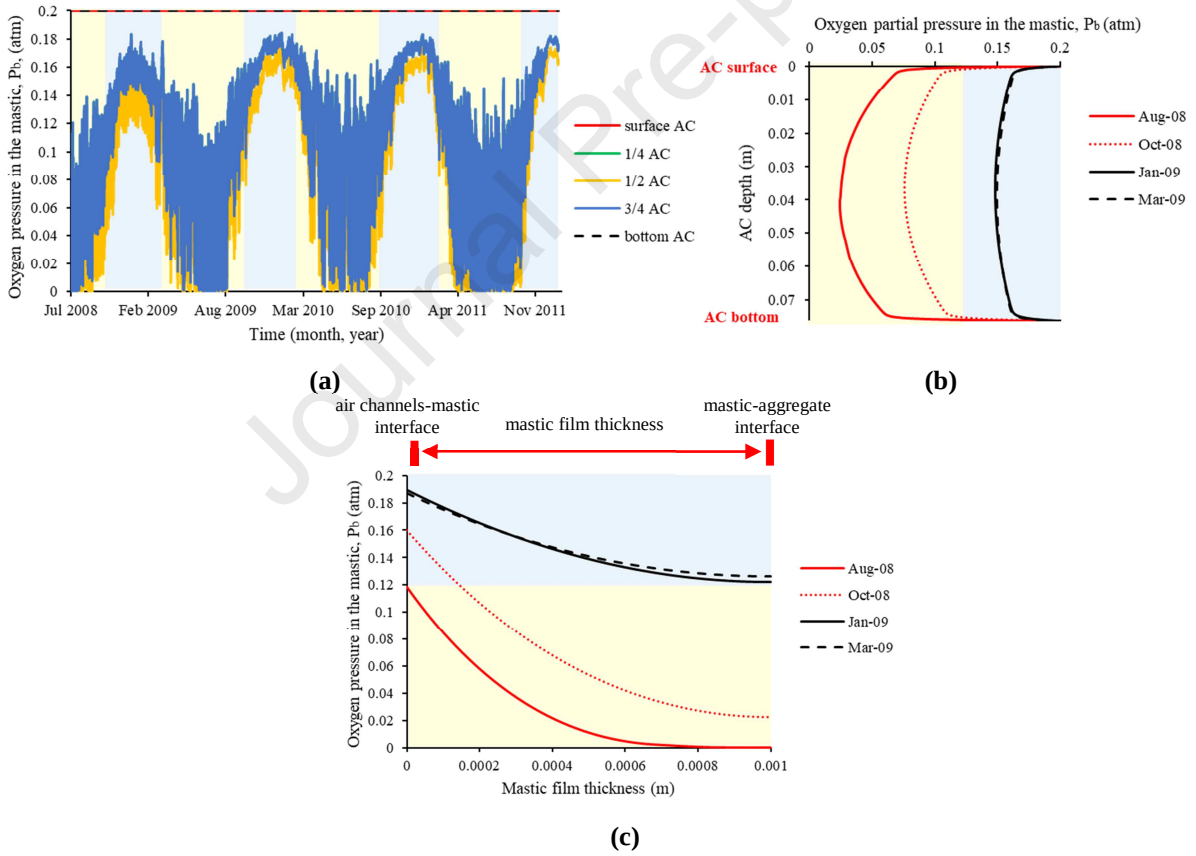

Fig. 11 Oxygen partial pressure distribution in the mastic for road section US277, located in Laredo, Texas, USA. (a) Oxygen partial pressure in the mastic plotted against ageing time at different AC depths (surface, ¼ AC, ½ AC, ¾ AC, and bottom AC layer), at points located at 1/3 the mastic thickness. (b) Oxygen pressure in the mastic plotted against depth of AC layer at different time intervals for points located at 1/3 the mastic thickness. (c) Oxygen partial pressure distribution in the mastic plotted against width of mastic coating film at different field ageing times at 1/3 AC depth. Winter and summer seasons are highlighted in blue and yellow colours, respectively.

Since the coefficient of oxygen diffusion inside the mastic is low, the oxygen pressure distribution will be non-uniform along the mastic film thickness at any time interval (when $t > 0$). As shown in **Figure 11 (c)**, the oxygen pressure is higher at the air-mastic interface but decreases horizontally along the mastic thickness toward the mas-

tic-aggregate interface. The non-uniform distribution of the oxygen pressure along the film thickness suggests that the carbonyl area growth will follow a similar pattern even if the temperature is constant across the mastic film thickness.

Moreover, the coefficient of oxygen diffusion D_o is inversely proportional to the carbonyl content (as illustrated in **Equations 8** and **9**). Therefore, it will decline with ageing time, as shown in **Figure 12**. This suggests that oxygen diffusion will limit the oxidation process gradually with progressive ageing. **Figure 12** also shows that the coefficient of oxygen diffusion changes periodically with temperature due to the fact that oxygen diffusivity in the mastic is highly associated with the viscosity of the binder, which is affected by temperature and oxidative hardening. Therefore, neglecting the ageing effect, the oxygen diffusivity would be expected to be higher in summer due to low apparent viscosity and lower in winter when high apparent viscosity is high. However, when considering the ageing effect, as shown in **Figure 12**, the coefficient of oxygen diffusion decreases in summer due to the increase in CA and maintains a relatively constant value during winter due to the lack of oxygen consumption.

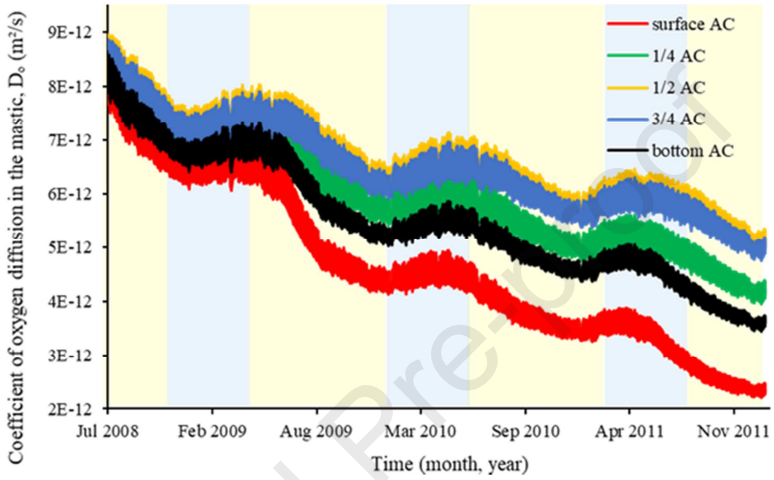

Fig. 12 Coefficient of oxygen diffusion in the mastic plotted against ageing time at different AC depths (surface, ¼ AC, ½ AC, ¾ AC, and bottom of AC layer) for road section US277, located in Laredo, Texas, USA. Points are located at 1/3 the mastic thickness. Winter and summer seasons are highlighted in blue and yellow colours, respectively.

6.4 Carbonyl Area at the Air Channels-Mastic Interface

The bitumen at the air-mastic interface is in direct contact with the oxygen in the air channels; therefore, it experiences more ageing than the bitumen at the same pavement depth inside the mastic film. Carbonyl production at this location depends on the oxygen pressure in the air channels. Therefore domain 1 (illustrated in **Figure 1**) was employed to measure CA at the air channels-mastic interface. Results for the CA growth with time at different depths are shown in **Figure 13(a)**. The growth pattern of the CA was affected by both temperature and oxygen pressure changes, displaying a faster growth rate in summer and a slower (or zero) growth rate in winter. This behaviour is attributed to the accelerated oxidation due to high temperatures in summer, leading to faster generation of carbonyl. Moreover, carbonyl growth declines with field ageing time, as a result of decreased oxygen diffusivity due to the increase in CA and oxidation hardening in the mastic. **Figure 13 (b)** shows that the CA pattern with depth forms an unsymmetrical C-shaped curve with higher CA values at the surface and the bottom of the AC layer and lower CA values in the middle of the AC layer. This pattern follows that of the oxygen pressure distribution in the air channels but with slightly higher CA values at the top surface than at the bottom due to higher surface temperatures that result in higher oxidative reactions. **Figure 13** shows that, compared to deeper asphalt layers, the AC surface layer ages severely due to high temperatures and complete availability of oxygen.

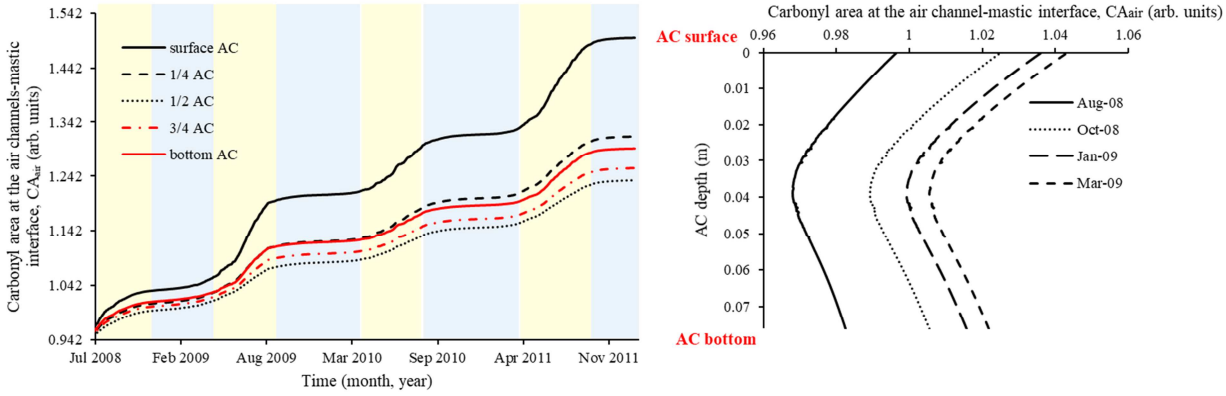

(a) (b)

Fig. 13 Carbonyl area at the air channels-mastic interface for road section US277, located in Laredo, Texas, USA. (a) Carbonyl area plotted against ageing time at different AC depths (surface, ¼ AC, ½ AC, ¾ AC, and bottom of AC layer). Winter and summer seasons are highlighted in blue and yellow colours, respectively. (b) Carbonyl area plotted against depth of AC at different ageing times.

6.5 Carbonyl Area in the Asphalt Mastic

Predicted carbonyl growth in the asphalt mastic coating film is compared with field measurements for road sections US277 and US83 in **Section 7**, while predicted results for road section US277 are detailed here. **Figure 14 (a** and **b)** shows that the carbonyl growth in the mastic follows the same pattern as that at the air-mastic interface; namely, the carbonyl grows quickly in summer due to high temperatures but increases at a very slow or zero rate in winter. The carbonyl area at the surface and bottom is higher than that in the middle due to high oxygen availability at the surface and bottom, leading to the C-shaped curve of the carbonyl profile along the pavement depth, as shown in Figure 14 (b). The CA values in the asphalt mastic are much less than those at the air-mastic interfaces, at the same pavement depth, although they have the same temperature profile. This observation shows that the availability of oxygen constrains carbonyl growth.

Figure 14 (c) shows the carbonyl area across the mastic coating film thickness at a certain depth of the AC layer (1/3 AC depth). CA is not produced equally across the width of the mastic coating film but decreases quickly along the film thickness moving away from the air-mastic interface. This observation is particularly important when calculating the average carbonyl area at a certain pavement depth. As shown in the simplified air/mastic structure in **Figure 2,** the perimeter of asphalt mastic surrounding the air channels is much less than that in contact with the aggregate. This materials distribution should be considered when calculating the average carbonyl area at a certain pavement depth.

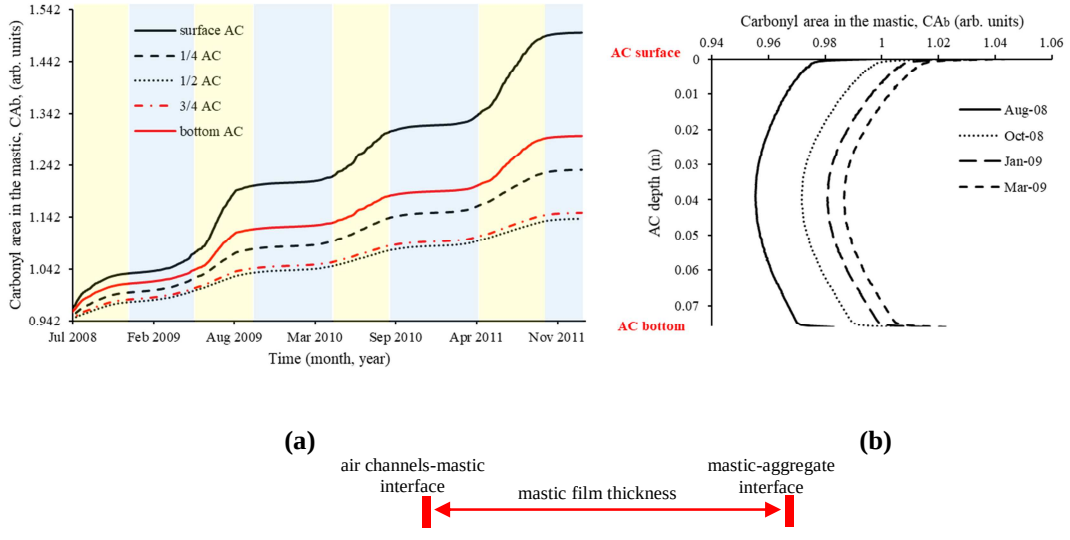

(a) (b)

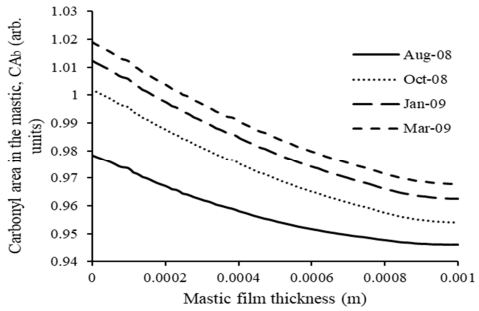

(c)

Fig. 14 Carbonyl area in the mastic (CA_b) for road section US277, located in Laredo, Texas, USA. (a) CA_b plotted against ageing time at different AC depths (surface, ¼ AC, ½ AC, ¾ AC, and bottom of AC layer), at points located at 1/3 the mastic thickness. Winter and summer seasons are highlighted in blue and yellow colours, respectively. (b) Carbonyl area in the mastic plotted against depth of AC layer at different time intervals. Points are located at 1/3 the mastic thickness. (c) Carbonyl area in the mastic plotted against thickness of mastic coating film at different field ageing times at 1/3 AC depth.

7 Field Validation of the Ageing Prediction Model

To verify the ageing predictions model, predicted carbonyl area values were compared with measurements of the binder extracted from field cores. The FHWA reports show that the cores were obtained from field sections at various ageing intervals. Cores were assembled and analysed for air voids percentage and accessible air voids by using air voids determination procedures and X-ray CT scans; then binders were extracted and recovered from sliced asphalt concrete samples at different pavement depths. The recovered binders were then analysed for oxidation products, specifically the carbonyl area using FTIR. This process is illustrated in **Figure 15** [17, 31, 33].

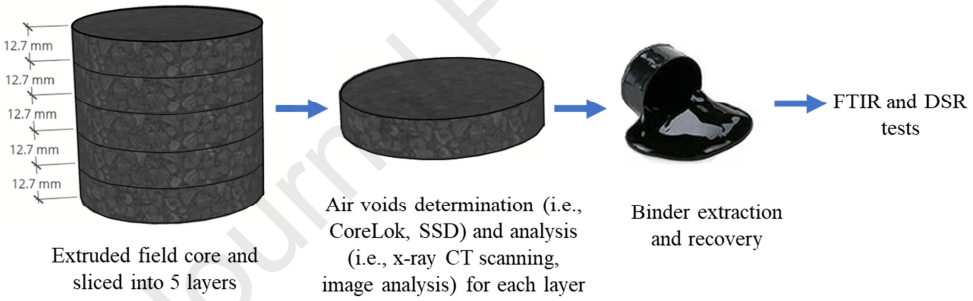

Fig. 15 Illustration of field sample extraction and binder recovery processes

The measured CA at a specific pavement depth is an overall representation of the carbonyl contents of the sliced asphalt samples at the specific pavement depth. It is necessary to calculate the average CA from the model predictions at the specific pavement depth to compare it with the measured CA for model validation. There are are two factors to consider when determining the average predicted CA at any depth of the AC layer: (1) The oxygen diffusion depth is employed based on the model illustrated in **Figure 2** such that oxygen diffuses horizontally in a hollow cylinder from the air channel along the mastic coating thickness toward the mastic-aggregate interface; (2) The carbonyl area is decreasing and non-uniformly distributed across the mastic film thickness (as shown in **Figure 14 (c)**). Therefore, the volumetric integration in **Equation 37** was adopted to calculate the average predicted carbonyl area at a certain depth.

$$CA_y = \frac{\int_{r_{air}}^{R} 2\,\pi CA(r)\,r\,dr}{\pi\,(R^2 - r_{air}^2)} \quad (37)$$

where CA_y is the average predicted carbonyl area at a certain depth of the AC layer (y), $CA(r)$ is the predicted carbonyl area at a radius of (r), r is the radius calculated from the centre of the air channels, the minimum radius would be the radius of the air channels (r_{air}), and the maximum radius would be the radius of the air channels plus the oxygen diffusion depth (d_D) in the mastic coating film, i.e., $R = r_{air} + d_D$.

The average predicted carbonyl area was obtained for each sliced AC sample at different pavement depths using **Equation 37** and compared against the field measurements. **Figure 16** shows a comparison between the pre-

dicted carbonyl content and the carbonyl content measured in the field for cores recovered at the wheel path. The field data seem to have unsystematic patterns across the pavement depth; for example, the field measurements of CA for road section US277 form an S-shape across the pavement depth. Nonetheless, in general, there is a meaningful agreement between the field measurements and the predicted values obtained by the comprehensive oxidative ageing models, and the predicted carbonyl profile shows a consistent increase with ageing year and a C-shaped curve along the pavement depth.

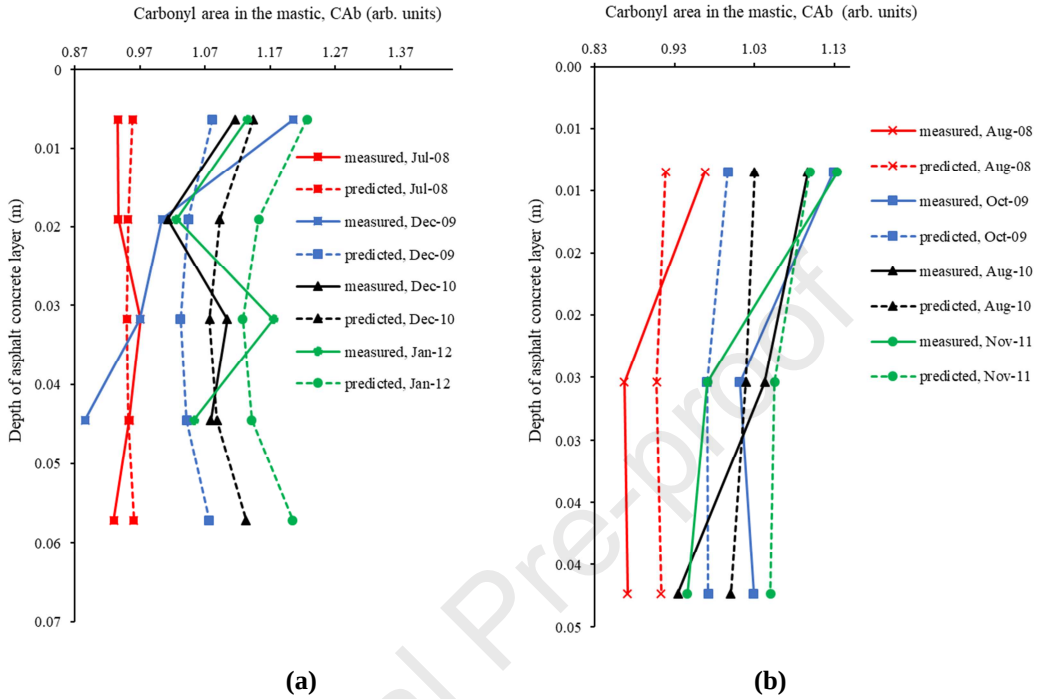

(a) **(b)**

Fig. 16 Comparison between the carbonyl area of recovered field cores and the predicted carbonyl area in the mastic (CA_b) obtained from the proposed oxidative ageing models (a) for road section US277 in Laredo, Texas, USA; (b) for road section US83 in Childress, Texas, USA.

8 Conclusions

This study proposes an equation-based multiphysics model to predict oxidative field ageing in asphalt pavements. The model predicts the pavement temperature profile, the oxygen pressure distribution in the accessible air channels, the oxygen pressure distribution in the asphalt mastic coating film, and the carbonyl area growth within the mastic coating film across pavement depth for three or more service years. The model requires location-specific hourly climate inputs, oxidation kinetics inputs obtained from ageing, rheological and chemical laboratory tests, and mixture volumetric properties derived from mix design specifications.

The proposed comprehensive ageing model was validated using field measurements of the oxidation products (the carbonyl area) for two road sections located in Texas, USA. By comparing the predictions with the carbonyl area from field samples collected by the FHWA, the conclusions are summarised as follows:

1. The model can effectively address the circular dependency among ageing-related multiphysics (i.e., heat transfer, oxygen diffusion, and oxidation kinetics). PDE-based FEM can reliably predict annual hourly profiles of temperature, oxygen pressure, and oxidation products growth across the pavement depth, in different climate zones.
2. The model overcomes some of the encountered uncertainties in oxidative ageing prediction. For instance, it relays more on site-specific climatic data, such as albedo, emissivity, and subsurface soil temperatures; and it doesn't require field calibration factor fcf to calibrate oxygen diffusion process in pavement. Moreover, the heat transfer model was calibrated to predict temperature profile in regions susceptible to freezing.
3. Oxygen pressure within the asphalt structure frequently changes due to seasonal and daily temperature variation, and it is affected by the oxidation process. Oxygen pressure becomes low with high daily flocculation during summer because asphalt mastic ages and consumes more oxygen when subjected to high temperatures. In contrast, oxygen pressure becomes high with low daily flocculation in winter,

because there is a low oxidation rate in this season due to low temperatures. This unique behaviour cannot be observed without using circular-dependent multiphysics model.

4. Design and materials selection of pavement directly impacts the severity and extend of oxidative ageing. For example, carbonyl area distribution takes C-shaped curve along AC depth (high oxidation rate at top and bottom boundaries), in case there is free air-accessibility though the underlying layer. If the underlying layer is inaccessible to air, such as cement/asphalt treated base, carbonyl area will be high at AC surface and low at bottom. Not to forget that this pattern is also affected by temperature profile, which causes irregular or different carbonyl area distribution pattern along pavement depth. Another example on the impact of pavement structure on oxidative ageing is the effect of interconnected air channels. Presence of accessible air channels is proportional with oxidation rate (i.e., the higher the radius and number of air channels, the higher the exposed surface area of mastic to air, and the higher the ageing rate).
5. There has been a long debate regarding the uniformity and distribution of oxidative ageing products along pavement depth. Modelling results in this study support that oxidative ageing is non-uniform and decreasing in general across pavement depth because it is highly sensitive to oxygen pressure and temperature profiles.

Future studies will cover the effect of climate region, oxidation kinetics, pavement structure, and binder modifiers on the severity of oxidative ageing in asphalt binders. The proposed model will be coupled with mechanical performance models to predict the mechanical response of asphalt pavements under the influence of long-term oxidative ageing.

9 Acknowledgement

The authors would like to gratefully acknowledge the financial support from Schlumberger Foundation: Faculty for the Future Fellowship program, and that from the European Commission's Horizon 2020 programme via a Marie S. Curie Individual Fellowship (Grant No. 749232).

Authors Contribution

The authors confirm contribution to the paper as follows: simulation work, data collection and analysis, and paper draft: Eman Omairey; paper draft, data collection, and paper review: Fan Gu; study conception, objective design, and paper review: Yuqing Zhang. All authors reviewed the results and approved the final version of the manuscript.

References

1. Petersen, J.C., 2000. Chemical composition of asphalt as related to asphalt durability. In Developments in petroleum science (Vol. 40, pp. 363-399). Elsevier.

2. Gao, Y., Zhang, Y., Gu, F., Xu, T. and Wang, H., 2018. Impact of minerals and water on bitumen-mineral adhesion and debonding behaviours using molecular dynamics simulations. *Construction and Building Materials*, *171*, pp.214-222.

3. Mirza, M.W., 1995. Development of a global aging system for short and long term aging of asphalt cements.

4. Airey, G.D., 2003. State of the art report on ageing test methods for bituminous pavement materials. International Journal of Pavement Engineering, 4(3), pp.165-176.

5. Petersen, J.C., 2009. A review of the fundamentals of asphalt oxidation. Transportation Research Circular.

6. Zhao, Y., Gu, F., Xu, J. and Jin, J., 2010. Analysis of aging mechanism of SBS polymer modified asphalt based on Fourier transform infrared spectrum. Journal of Wuhan University of Technology-Mater. Sci. Ed., 25(6), pp.1047-1052.

7. Omairey, E.L., Zhang, Y., Al-Malaika, S., Sheena, H. and Gu, F., 2019. Impact of anti-ageing compounds on oxidation ageing kinetics of bitumen by infrared spectroscopy analysis. Construction and Building Materials, 223, pp.755-764.

8. Yang, Y., Zhang, Y., Omairey, E., Cai, J., Gu, F. and Bridgwater, A.V., 2018. Intermediate pyrolysis of organic fraction of municipal solid waste and rheological study of the pyrolysis oil for potential use as bio-bitumen. *Journal of cleaner production*, *187*, pp.390-399.

9. Liu, M., Lunsford, K.M., Davison, R.R., Glover, C.J. and Bullin, J.A., 1996. The kinetics of carbonyl formation in asphalt. AIChE Journal, 42(4), pp.1069-1076.

10. Jin, X., Han, R., Cui, Y. and Glover, C.J., 2011. Fast-rate–constant-rate oxidation kinetics model for asphalt binders. Industrial & Engineering Chemistry Research, 50(23), pp.13373-13379.

11. Petersen, J.C. and Harnsberger, P.M., 1998. Asphalt aging: dual oxidation mechanism and its interrelationships with asphalt composition and oxidative age hardening. Transportation Research Record, 1638(1), pp.47-55.

12. Luo, X., Gu, F. and Lytton, R.L., 2015. Prediction of field aging gradient in asphalt pavements. Transportation Research Record, 2507(1), pp.19-28.

13. Luo, X., Gu, F. and Lytton, R.L., 2019. Kinetics-based aging prediction of asphalt mixtures using field deflection data. International Journal of Pavement Engineering, 20(3), pp.287-297.

14. Al-Rub, R.K.A., Darabi, M.K., Kim, S.M., Little, D.N. and Glover, C.J., 2013. Mechanistic-based constitutive modeling of oxidative aging in aging-susceptible materials and its effect on the damage potential of asphalt concrete. Construction and Building Materials, 41, pp.439-454.

15. Yin, F., Martin, A.E., Arámbula-Mercado, E. and Newcomb, D., 2017. Characterization of non-uniform field aging in asphalt pavements. Construction and Building Materials, 153, pp.607-615.

16. Prapaitrakul, N., Han, R., Jin, X. and Glover, C.J., 2009. A transport model of asphalt binder oxidation in pavements. Road Materials and Pavement Design, 10(sup1), pp.95-113.

17. Jin, X., Cui, Y. and Glover, C.J., 2013. Modeling asphalt oxidation in pavement with field validation. Petroleum Science and Technology, 31(13), pp.1398-1405.

18. Lytton, R.L., Pufahl, D.E., Michalak, C.H., Liang, H.S. and Dempsey, B.J., 1993. An integrated model of the climatic effects on pavements.

19. Han, R., Jin, X. and Glover, C.J., 2011. Modeling pavement temperature for use in binder oxidation models and pavement performance prediction. Journal of Materials in Civil Engineering, 23(4), pp.351-359.

20. Lu, X. and Isacsson, U., 1998. Chemical and rheological evaluation of ageing properties of SBS polymer modified bitumens. Fuel, 77(9-10), pp.961-972.

21. Wang, P.Y., Wen, Y., Zhao, K., Chong, D. and Wong, A.S., 2014. Evolution and locational variation of asphalt binder aging in long-life hot-mix asphalt pavements. *Construction and Building Materials*, *68*, pp.172-182.

22. Lu, X. and Isacsson, U., 2002. Effect of ageing on bitumen chemistry and rheology. Construction and Building materials, 16(1), pp.15-22.

23. Jing, R., Varveri, A., Liu, X., Scarpas, A. and Erkens, S., 2019. Rheological, fatigue and relaxation properties of aged bitumen. *International Journal of Pavement Engineering*, pp.1-10.

24. Ruan, Y., Davison, R.R. and Glover, C.J., 2003. Oxidation and viscosity hardening of polymer-modified asphalts. Energy & fuels, 17(4), pp.991-998.

25. Luo, X., Zhang, Y. and Lytton, R.L., 2016. Implementation of pseudo J-integral based Paris' law for fatigue cracking in asphalt mixtures and pavements. *Materials and Structures*, *49*(9), pp.3713-3732.

26. Zhang, Y., Luo, R. and Lytton, R.L., 2014. Anisotropic characterization of crack growth in the tertiary flow of asphalt mixtures in compression. Journal of Engineering Mechanics, 140(6), p.04014032.

27. Zhang, Y., Birgisson, B. and Lytton, R.L., 2015. Weak form equation–based finite-element modeling of viscoelastic asphalt mixtures. Journal of Materials in Civil Engineering, 28(2), p.04015115.

28. Multiphysics, C.O.M.S.O.L., 2013. Comsol multiphysics reference manual. COMSOL: Grenoble, France, p.1084.

29. Zhang, Y., Gu, F., Luo, X., Birgisson, B. and Lytton, R.L., 2018. Modeling Stress-Dependent Anisotropic Elastoplastic Unbound Granular Base in Flexible Pavements. *Transportation Research Record*, *2672*(52), pp.46-56.

30. Dickinson, E.J., 1984. The diffusion controlled reaction of oxygen with films of bituminous binders. Australian Road Research, 14(3).

31. Glover, C.J., Han, R., Jin, X., Prapaitrakul, N., Cui, Y., Rose, A., Lawrence, J.J., Padigala, M., Arambula, E., Park, E.S. and Martin, A.E., 2014. Evaluation of binder aging and its influence in aging of hot mix asphalt concrete: technical report (No. FHWA/TX-14/0-6009-2). Texas. Dept. of Transportation. Research and Technology Implementation Office.

32. Vehrencamp, J.E., 1953. Experimental investigation of heat transfer at an air□Earth interface. *Eos, Transactions American Geophysical Union*, *34*(1), pp.22-30.

33. Han, R., 2011. Improvement to a transport model of asphalt binder oxidation in pavements: Pavement temperature modeling, oxygen diffusivity in asphalt binders and mastics, and pavement air void characterization. Texas A&M University.

34. Wen, Y. and Wang, Y., 2018. Determination of oxygen diffusion coefficients of compacted asphalt mixtures. Construction and Building Materials, 160, pp.385-398.

35. Luca, J. and Mrawira, D., 2005. New measurement of thermal properties of superpave asphalt concrete. Journal of Materials in Civil Engineering, 17(1), pp.72-79.

36. Highter, W., 1984. Thermal properties of some asphaltic concrete mixes. In International Air Transportation Conference (p. 1598).

37. Gui, J., Phelan, P.E., Kaloush, K.E. and Golden, J.S., 2007. Impact of pavement thermophysical properties on surface temperatures. Journal of materials in civil engineering, 19(8), pp.683-690.

38. Hassn, A., Aboufoul, M., Wu, Y., Dawson, A. and Garcia, A., 2016. Effect of air voids content on thermal properties of asphalt mixtures. Construction and Building Materials, 115, pp.327-335.

39. Hassn, A., Chiarelli, A., Dawson, A. and Garcia, A., 2016. Thermal properties of asphalt pavements under dry and wet conditions. Materials & Design, 91, pp.432-439.

40. Bai, B.C., Park, D.W., Vo, H.V., Dessouky, S. and Im, J.S., 2015. Thermal properties of asphalt mixtures modified with conductive fillers. Journal of Nanomaterials, 16(1), p.255.

41. Nguyen, Q.T., Di Benedetto, H. and Sauzéat, C., 2012. Determination of thermal properties of asphalt mixtures as another output from cyclic tension-compression test. Road Materials and Pavement Design, 13(1), pp.85-103.

42. Yavuzturk, C., Ksaibati, K. and Chiasson, A.D., 2005. Assessment of temperature fluctuations in asphalt pavements due to thermal environmental conditions using a two-dimensional, transient finite-difference approach. Journal of Materials in Civil Engineering, 17(4), pp.465-475.

43. Pan, P., Wu, S., Hu, X., Liu, G. and Li, B., 2017. Effect of material composition and environmental condition on thermal characteristics of conductive asphalt concrete. Materials, 10(3), p.218.

44. Alavi, M., Hajj, E.Y. and Sebaaly, P.E., 2017. A comprehensive model for predicting thermal cracking events in asphalt pavements. International Journal of Pavement Engineering, 18(9), pp.871-885.

45. Chen, J., Zhang, M., Wang, H. and Li, L., 2015. Evaluation of thermal conductivity of asphalt concrete with heterogeneous microstructure. Applied Thermal Engineering, 84, pp.368-374.

46. Alawi, M.H. and Helal, M.M., 2014. A mathematical model for the distribution of heat through pavement layers in Makkah roads. Journal of King Saud University-Engineering Sciences, 26(1), pp.41-48.

47. Shi, X., 2014. Controlling thermal properties of asphalt concrete and its multifunctional applications (Doctoral dissertation).

48. Martin, A.E., Arambula, E., Kutay, M.E., Lawrence, J., Luo, X. and Lytton, R., 2013. Comparison of fatigue analysis approaches for hot-mix asphalt to ensure a state of good repair (No. SWUTC/13/600451-00012-1). Southwest Region University Transportation Center (US).

49. Sebesta, S., Scullion, T. and Von Holdt, C., 2006. Rubblization for Rehabilitation of Concrete Pavement in Texas: Preliminary Guidelines and Case Studies (No. FHWA/TX-06/0-4687-1). Texas Transportation Institute, Texas A & M University System.

- PDE-based FE model is developed to predict oxidative ageing of asphalt pavements.
- The model effectively addresses the circular dependency among ageing multiphysics.
- Temperature profile prediction model is modified to be location-dependent.
- Oxidative ageing is non-uniform (decreasing) along asphalt pavement depth.
- Oxygen distribution in pavement changes with CA content and temperature.

To Journal of Cleaner Production,
12 May 2020

Statement of Conflict of Interest

Re: submission of paper entitled "An Equation-Based Multiphysics Modelling Framework for Oxidative Ageing of Asphalt Pavements" by Eman L. Omairey, Fan Gu, and Yuqing Zhang to Journal of Cleaner Production.

We (all authors) wish to confirm that there are no known conflicts of interest associated with this publication, and there has been no significant financial support for this work that could have influenced its outcome.

We confirm that the manuscript has been read and approved by all named authors and that there are no other persons who satisfied the criteria for authorship but are not listed. We further confirm that the order of authors listed in the manuscript has been approved by all of us.

We confirm that we have given due consideration to the protection of intellectual property associated with this work and that there are no impediments to publication, including the timing of publication, with respect to intellectual property. In doing so, we confirm that we have followed the regulations of our institutions concerning intellectual property.

We understand that the Corresponding Author is the sole contact for the Editorial process (including Editorial Manager and direct communications with the office). He is responsible for communicating with the other authors about progress, submissions of revisions and final approval of proofs.

We confirm that we have provided a current, correct email address which is accessible by the Corresponding Author and which has been configured to accept email.

Sincerely yours,

Signed by Corresponding Author on behalf of all authors.

Yuqing Zhang, PhD
Senior Lecturer in Highway Engineering
Aston Institute of Materials Research (AIMR)
Engineering System & Management (ESM)
Aston University
Address: Aston Triangle, Birmingham, B4 7ET, U.K.
Tel: +44 121-204-3391
Email: y.zhang10@aston.ac.uk